

# **MODIFICATION OF GRAPHENE SURFACES FOR DETECTION OF BIOMICROPARTICLES**

**A Thesis Submitted to  
the Graduate School of Engineering and Sciences of  
İzmir Institute of Technology  
in Partial Fulfillment of the Requirements for the Degree of**

**MASTER OF SCIENCE**

**in Biotechnology**

**by  
Gözde YEŞİLTAŞ**

**December 2019  
İZMİR**

We approve the thesis of Gözde YEŞİLTAS

Examining Committee Members:



Prof. Dr. Volpa BULMUŞ  
Department of Bioengineering, İzmir Institute of Technology

Assoc. Prof. Dr. Müjdat BALANTEKİN  
Department of Electrical and Electronics Engineering, İzmir Institute of Technology



Assist. Prof. Dr. Gizem KALELİ ÇAN  
Department of Biomedical Engineering, İzmir Democracy University

20 December 2019



Prof. Dr. Volga BULMUŞ  
Supervisor, Department of  
Bioengineering  
İzmir Institute of Technology



Prof. Dr. Gülşah ŞANLI MOHAMED  
Head of the Department of Biotechnology  
and Bioengineering



Prof. Dr. Mehtap EMIRDAG EANES  
Dean of the Graduate School of  
Engineering and Sciences

## ACKNOWLEDGMENTS

Firstly, I would like to express my endless thanks to my supervisor Prof. Dr. Volga Bulmuş for her support, direction and the most importantly the chance she has given me to work with her laboratory team. Throughout my thesis studies, I have learned so much from her and also it has been an honor and happiness to me to experiment with her.

I also would like to thank to Assist. Prof. Dr. Hadi Zareie for giving the opportunity to work with his lab team and for experimental aids.

I would like to acknowledge TÜBİTAK for financial support through PROJECT NO: 117F186.

I would like to thank to Assist. Prof. Dr. Müjdat Balantekin for giving the opportunity to study at this project. In the thesis, for providing the Jurkat cells that used I would like to thank Prof. Dr. Yusuf Baran and his team. In addition, I would like to thank to Assoc. Prof. Cem Çelebi and his team for providing graphene surfaces that used.

I would also like to thank Aysel Tomak for her assistance with experiments and her valuable help with all matters. I am most grateful to my labmates; Aysel Tomak, Aytaç Gül, Damla Taykoz, Aykut Zelçak, Cansu Söylemez, İlayda Özkan, Gürbüz Dursun and Fazilet Akay. They deserve the biggest thanks for their help and support throughout my M.Sc. study.

Also, I would like to thank the staff of Biotechnology and Bioengineering Research and Application Center for their help and support throughout the experiments in BIOMER.

I am warmly thankful to my close friends Banu Biltekin, İsmail Tahmaz, Ayşe Nur Akin, Merve Arpacıoğlu and Çağlar Çil for sustained encouragements to be social, help and guide.

Lastly and most importantly, I thank my family for supporting me during all my education and social life. I am grateful of my father İbrahim Yeşiltaş, my brother Gökhan Yeşiltaş and of course my dear mother Ayşe Yeşiltaş for their endless love, support and patience during my thesis and all life.

# ABSTRACT

## MODIFICATION OF GRAPHENE SURFACES FOR DETECTION OF BIOMICROPARTICLES

Pathogens present in the food we consume and the water we drink pose a major threat to human health. Another major health concern is the metastasis of cancer in which cancer cells spread to new areas of the body, often by way of the lymph system or bloodstream. To minimize the burden on health and economy, the detection of biomicroparticles such as pathogens or circulating cancer cells in a highly sensitive and practical manner is highly desirable. This thesis aims to develop a method to create graphene-based biosensor substrate for detection of biomicroparticles such as bacteria, viruses or mammalian cells.

For this aim, graphene surface was first functionalized using a linker molecule. The effect of solvent type on functionalization was investigated via Raman spectroscopy and X-Ray spectroscopy (XPS). AntiCD2 antibodies (Ab), as a model antibody, were then conjugated to the functionalized graphene via NHS/EDC chemistry. The Ab conjugation was verified by Raman spectroscopy and XPS analyses. Finally, Jurkat cells, as model biomicroparticles, were recognized and captured by Ab-conjugated graphene surface, as evidenced by optical microscopy. The temperature, medium, and method for interaction of cells with graphene surfaces as well as the specificity of the Ab- functionalized graphene surface were investigated. The results overall showed the specific and efficient recognition of model cell line by Ab-conjugated graphene surfaces.

**Keywords :** Biosensor, Graphene, Antibody, Cell capture, Biomicroparticle.

## ÖZET

### BIYOMİKROPARTİKÜLLERİN BELİRLENMESİ İÇİN GRAFEN YÜZEYLERİN MODİFİKASYONU

Tükettiğimiz yiyeceklerde ve içtiğimiz sularda bulunan patojenler insan sağlığı için büyük bir tehdit oluşturmaktadır. Bir diğer önemli sağlık sorunu, kanser hücrelerinin genellikle lenf sistemi veya kan dolaşımı yoluyla vücudun yeni bölgelerine yayıldığı kanser metastazıdır. Sağlık ve ekonomi üzerindeki yükü en aza indirmek için, patojenler veya dolaşımdaki kanser hücreleri gibi biyomikropartiküllerin oldukça hassas ve pratik bir şekilde saptanması talep edilen bir durumdur. Bu tez, bakteri, virüs veya memeli hücresi gibi biyomikropartiküllerin tespiti için grafen esaslı biyosensör substratı oluşturmak için bir yöntem geliştirmeyi amaçlamaktadır.

Bu amaçla grafen yüzey ilk olarak bir bağlayıcı ara molekül kullanılarak fonksiyonelleştirildi. Çözücü tipinin grafen yüzey fonksiyonelleştirilmesi üzerindeki etkisi Raman spektroskopisi ve X-Ray spektroskopisi (XPS) ile araştırıldı. Daha sonra bir model antikor olarak AntiCD2 antikoru (Ab), NHS / EDC kimyası yoluyla fonksiyonelleştirilmiş grafen yüzeye konjüge edildi. Ab konjugasyonu Raman spektroskopisi ve XPS analizleriyle tespit edilmiştir. Son olarak, model biyomikropartiküller olarak kullanılan Jurkat hücreleri, Ab ile konjüge grafen yüzeyi tarafından tanındı ve hücre-yüzey etkileşimi optik mikroskopi ile kanıtlandı. Hücrelerin grafen yüzeyleri ile etkileşimi için sıcaklık, ortam ve yöntem ile Ab-fonksiyonel grafen yüzeyinin özgüllüğü araştırıldı. Sonuçlar genel olarak Ab-konjüge grafen yüzeyler tarafından model hücre hattının spesifik ve etkili bir şekilde tanınmasını gösterdi.

**Anahtar Sözcükler:** Biyosensör, Grafen, Antikor, Hücre tutma, Biyomikropartikül.

# TABLES OF CONTENTS

<u>LIST OF FIGURES.....</u>	<u>viii</u>
<u>LIST OF TABLES.....</u>	<u>xi</u>
CHAPTER 1. INTRODUCTION.....	1
CHAPTER 2. BACKGROUND.....	2
2.1. Graphene.....	2
2.2. Properties of Graphene.....	5
2.2.1. Electrical Properties.....	5
2.2.2. Mechanical Properties of Graphene.....	6
2.2.3. Optical Properties.....	7
2.2.4. Thermal Properties.....	7
2.2.5. Chemical Properties of Graphene.....	7
2.3. Graphene Based Biosensors Applications.....	8
2.4. Functionalization Strategies of Graphene Surface.....	13
2.4.1. Covalent Functionalization of Graphene.....	15
2.4.2. Non-Covalent Functionalization of Graphene.....	16
2.5. Antibody-Cell Receptor Interaction.....	17
CHAPTER 3. MATERIALS AND METHODS.....	20
3.1. Materials.....	20
3.2. Instruments.....	21
3.2.1. Raman Spectroscopy.....	21
3.2.2. X-Ray Photoelectron Spectroscopy (XPS).....	21
3.2.3. Stereo Microscope.....	21
3.3. Methods.....	22
3.3.1. Functionalization of Graphene Surfaces.....	22
3.3.2. Conjugation of Antibodies to Graphene Surfaces.....	22
3.3.3. Interaction of Antibody-Functionalized Graphene Surfaces with Cells.....	23

3.3.4. <u>Cell Culture</u> .....	23
CHAPTER 4. RESULTS AND DISCUSSION.....	24
4.1. <u>Functionalization of Graphene Surfaces</u> .....	24
4.2. <u>Antibody Conjugation to Functionalized Graphene</u> .....	28
4.3. <u>Recognition of Cells by Antibody Conjugated Graphene Surfaces</u> .....	31
CHAPTER 5. CONCLUSION.....	37
<u>FUTURE WORKS</u> .....	37
<u>REFERENCES</u> .....	40

## LIST OF FIGURES

<b><u>Figure</u></b>	<b><u>Page</u></b>
Figure 2.1. Representation of different carbon allotropes from a graphene surface layer [5].....	2
Figure 2.2. A) Graphite; and (B) Schematic demonstration of a single graphene layer from graphite [4].....	3
Figure 2.3. Number of annual publications of graphene and functionalized graphene [14].....	4
Figure 2.4. Schematic representation of a graphene platform and biosensor components [90].....	9
Figure 2.5. Representation of the most common attachment methods of bioreceptors [90].....	10
Figure 2.6. Schematic representation of graphene surface modified with antibodies for the recognition of pathogens [89].....	11
Figure 2.7. Schematic representation of graphene-based nanomaterials as a DNA biosensor Electrochemical detection (a) and fluorescence detection (b) [80].....	12
Figure 2.8. Schematic representation of the covalent and non-covalent functionalization of graphene [60].....	14
Figure 2.9. Schematic demonstration of the covalent (up) and non-covalent (down) functionalization of graphene [49,53].....	14
Figure 2.10. Representation of covalent modification of graphene surface with Diels Alder Reaction [49].....	15
Figure 2.11. Representation of covalent modification of graphene surface with organic cross-linkers [52].....	16
Figure 2.12. Schematic representation of pyrene derivatives used for non-covalently functionalization of graphene [57].....	17
Figure 2.13. Schematic representation of antibody structure. (A) Schematic representation of the X-ray crystallographic structure of an IgG antibody. (B) Schematic representation of the four-chain composition	

of the antibody structure and the domains containing each chain. (C) representation of a simplified form of an antibody molecule [65]. 18

Figure 4.1. Raman spectra of graphene surfaces after functionalization with PBA (10 mM) in different solvents (A) Ethanol and mixtures with DMF at different v:v ratios (B) Methanol and mixtures with DMF at different v:v ratios.....	25
Figure 4.2. C1s XPS spectra of graphene surfaces (A) non-functionalized (B) after functionalization with PBA using methanol (C) after functionalization with PBA using methanol:DMF (80:20) (D) after functionalization with PBA using methanol : DMF (95: 5).....	26
Figure 4.3. C1s XPS spectra of the functionalized graphene surface (A) Spectrum of the non-functionalized graphene surface (B) Spectrum of the PBA-functionalized surface (C) Spectrum of the PBA-functionalized surface activated with Ab directly (D) Spectrum of the antibody-conjugated graphene surface.....	29
Figure 4.4. N1s XPS spectra of the functionalized graphene surfaces and non-functionalized graphene surface.....	30
Figure 4.5. Effect of temperature on cell interaction with graphene surfaces in PBS for 1 hour by dipping method. Optical microscope images of (A) nonfunctionalized graphene surface after interaction with cells at 4° C, (B) nonfunctionalized graphene surface after interaction with cells at 37° C, (C) PBA-functionalized graphene surface after interaction with cells at 4° C, (D) PBA-functionalized graphene surface after interaction with cells at 37° C, (E) Ab-conjugated graphene surface after interaction with cells at 4° C, (F) Ab-conjugated graphene surface after interaction with cells at 37° C.....	32
Figure 4.6. Effect of method on cell interaction with graphene surfaces in PBS at 4°C for 1 hour. Optical microscope images of (A) PBA-functionalized graphene surface after interaction with cells via dropping method, (B) PBA-functionalized graphene surface after interaction with cells via	

dipping method, (C) Ab-conjugated graphene surface after interaction with cells by dropping method, (D) Ab-conjugated graphene surface

	after interaction with cells by dipping method.....	33
Figure 4.7.	Effect of medium on cell interaction with graphene surfaces at 4°C for 1 hour via dipping method. Optical microscope images of (A) PBA-functionalized graphene surface after interaction with cells in PBS, (B) PBA-functionalized graphene surface after interaction with cells in cell culture medium, (C) Ab-conjugated graphene surface after interaction with cells in PBS, (D) Ab-conjugated graphene surface after interaction with cells in cell culture medium.....	34
Figure 4.8.	Optical microscope images of (A) antiCD2 antibody-conjugated graphene surface after interaction with Jurkat cells in PBS at 4°C for 1 hour via dipping method, (B) Anti-Syndecan-1 antibody-conjugated graphene surface after interaction with Jurkat cells in PBS at 4°C for 1 hour via dipping method.....	35
Figure 4.9.	Optical microscope images of antiCD2 antibody-conjugated graphene surfaces after interaction with Jurkat cells followed by the treatment with the antiCD2 antibody solution (30 µg/ml in PBS) for 1 hour at 4°C. (A) Before and (B) after treatment with the excess of antiCD2 antibody solution.....	36

## LIST OF TABLES

<b><u>Table</u></b>	<b><u>Page</u></b>
Table 2.1. Table of results obtained using AFM of mechanical properties of graphene [8].....	6
Table 4.1. Polarity index values of solvent systems tested for graphene-PBA interactions.....	24
Table 4.2. The average atomic percentage values of the Si2p, C1s and O1s of the graphene surfaces before and functionalization with PBA in different solvents.....	27
Table 4.3. The average atomic percentage values of the C1s and O1s normalized to the average atomic percentage values of the Si2p of the graphene surfaces before and functionalization with PBA in different solvents.....	28
Table 4.4. The ratio of the average atomic percentage values of C1s, N1s and O1s atoms to the mean atomic percentage values of Si2p.....	30

# CHAPTER 1

## INTRODUCTION

Studies on biosensors have spread over a wide range of applications including medicine, food and pharmaceutical industries. Biosensors are designed to provide accurate, fast, cheap and reliable results. Graphene is preferred in many biosensors applications because of its thermal conductivity, high mechanical strength, flexibility, electronic mobility, thermal stability, chemical stability and transparency properties. Detection of biomicroparticles such as pathogens or cancer cells is an important target in biosensor applications. This thesis aims to develop a method for creating a graphene based biosensor substrate for the detection of biomicroparticles such as mammalian cells. Accordingly, the first chapter of this thesis provides literature review on graphene as a material, graphene-based biosensors and functionalization methods of graphene. The third chapter describes the materials and methods used in this thesis. Briefly, the graphene surface was first functionalized with an intermediate molecule. The effect of solvent on functionalization was investigated by Raman spectroscopy and X-Ray spectroscopy (XPS). AntiCD2 antibodies (Ab) as a model antibody was then covalently conjugated with the functionalized graphene surface via EDC/NHS chemistry. Biomolecule conjugation was confirmed using Raman spectroscopy and XPS. Finally, Jurkat cells as model biomicroparticles were recognized by the Ab-activated graphene surface. The cell capturing was observed by optical microscopy. In addition to the specificity of the Ab-functionalized graphene surface towards Jurkat cells, the interaction temperature, medium and method were investigated. Chapter 4 presents the results and discussion achieved throughout the study. The results of this thesis showed that the model cell line was recognized specifically and efficiently by Ab-functionalized graphene surfaces. Chapter 5 gives conclusions of the presented research and future recommendations.

## CHAPTER 2

### BACKGROUND

#### 2.1. Graphene

Carbon-based materials are available in three-dimensional (3D) forms (considered allotrope) in diamond and graphite. The proof of the 3D graphite carbon form goes back to the 1500s [1,2]. In the 1980s and 1990s, other carbon allotropes of graphene, such as zero-dimensional (0D) fullerene [1] and one-dimensional (1D) carbon nanotubes

[2] were discovered and this allows the graphene to be used in different workspaces. Different carbon allotrops from a graphene layer demonstrate in Figure 2.1 However, until 2004, a debate on the presence of two-dimensional (2D) allotropic carbon continued; A publication published by Andre Geim and Konstantin Novoselov shows the division of highly ordered pyrolytic graphite (HOPG) when a single graphene layer (graphene) has been successfully isolated micromechanically on an adhesive tape (Scotch Tape Method) [4].

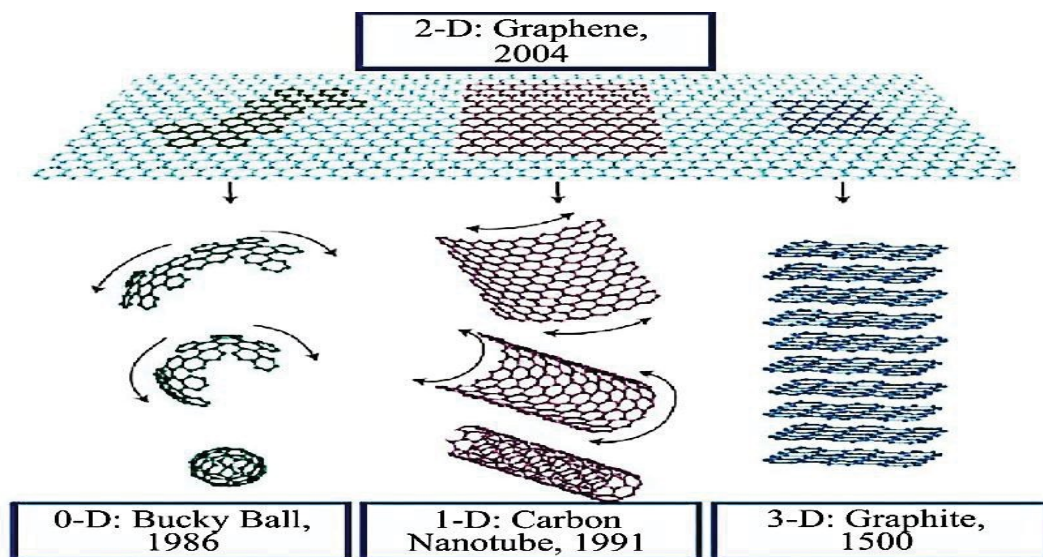


Figure 2.1. Representation of different carbon allotropes from a graphene surface layer [5].

The two-dimensional (2D) monolayer structure of covalently bonded  $sp^2$  hybridized carbon atoms is called graphene and graphene is a honeycomb form formed by carbon atoms [5].

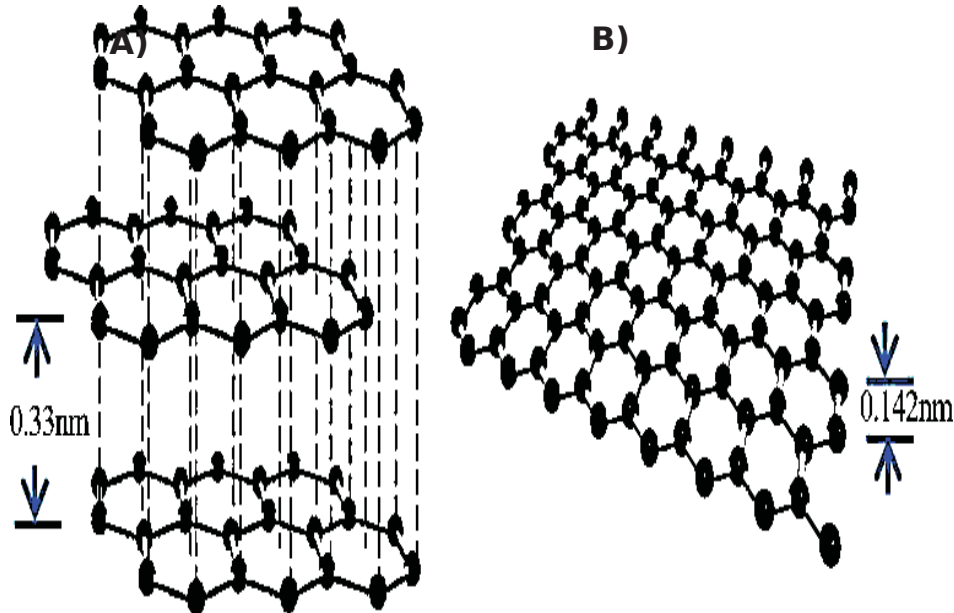


Figure 2.2. A) Graphite; and (B) Schematic demonstration of a single graphene layer from graphite [4].

The other carbon is the only atomic thick allotrope that acts as the basic structural unit for allotropic forms: 1) 0D, a sphere allotrope (Bucky ball), 2) 1D carbon nanotube form (CNT), performed by rolling a graphene layer. This rounding is carried out so that the carbon nanotubes form a cylindrical structure. 3) It is formed by stacking several separate layers of graphene layer held together by van der Waals bonds as in the structures of carbon shown in Figure 2.1 [5]. In general, single, double and triple graphite layers are widely used. These are known as monolayer, bilayer and triple graphene layers, respectively. Graphene layers exceeding 5 and 30 are generally referred to as multi-layer graphene / thick graphene [6]. The carbon atoms in the form of a honeycomb structure and attached to this structure have a bond length of 0.142 nm CC in the graphene structure. Furthermore, the height (thickness) between the layers is approximately 0.33 nm (3.3 Å) as shown in Figure 2.2 [3].

Graphene is advantageous in numerous studies because it has many remarkable properties such as a large theoretical specific surface area ( $2630 \text{ m}^2\text{g}^{-1}$ ) [7], high internal mobility ( $200,000 \text{ cm}^2 \text{ V}^{-1} \text{ s}^{-1}$ ) [8,9], high Young modulus value ( $\sim 1.0 \text{ TPa}$ ) [10], chemical properties and thermal conductivity ( $\sim 5000 \text{ Wm}^{-1}\text{K}^{-1}$ ) [11]. It is also able to

withstand good optical permeability ( $\sim 97.7\%$ ), good electrical conductivity and current density of  $108 \text{ \AA} / \text{cm}^2$ . Graphene is also known as zero-band semiconductor. Therefore, the band gap can be adjusted physicochemically. Because of these remarkable properties of graphene, researches on graphene and its derivatives in the field of materials science and condensed matter physics has attracted great attention in the last few years with various applications such as membrane nanoelectronics, Li-ion batteries, electrodes, supercapacitors, biosensors, and drug delivery.

Graphene is one of the most studied materials in recent years due to all the mentioned features [14,15]. In 2004, Geim and Nosovelov of the University of Manchester was succeeded in isolating a single layer of graphene. This ground breaking discovery and later work on the physics of graphene encouraged the authors to win the Nobel Prize in Physics in 2010 and the growth of graphene research involving various disciplines. Since graphene is carbon based, it provides opportunity for biological studies. The increase in graphene-based studies is shown in Figure 2.3 [16].

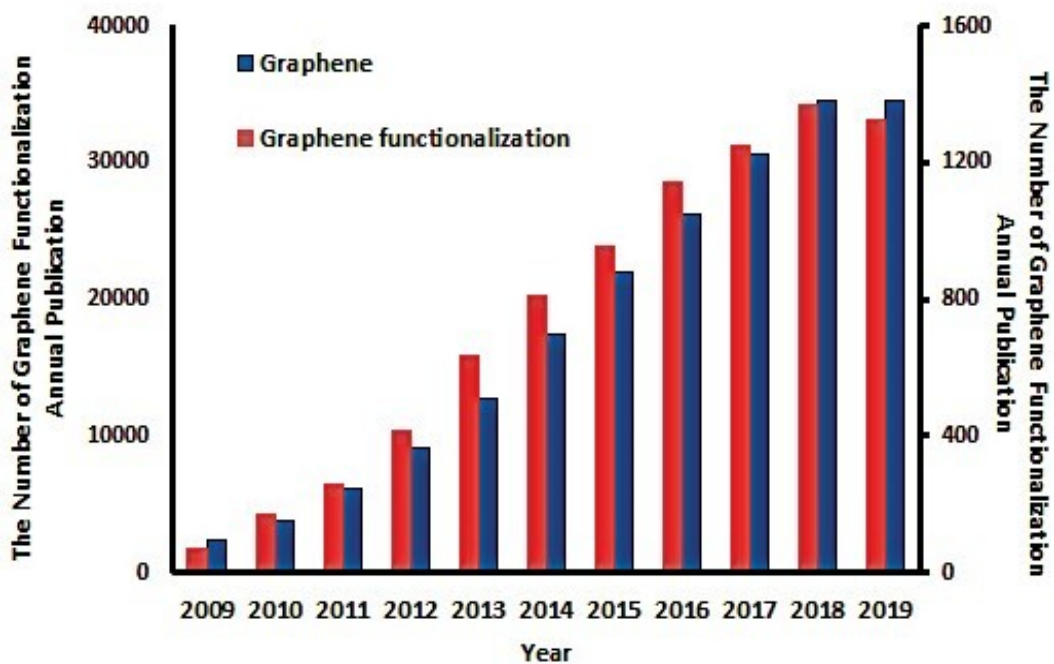


Figure 2.3. Number of annual publications of graphene and functionalized graphene [14].

Graphene is synthesized by micromechanical disintegration of graphite. Although it is a timeconsuming process and not suitable for mass-scale production, it can be synthesized in high quality pure [17]. Recently, for the synthesis of graphene, a number of different methods such as epitaxial growth by chemical vapour deposition on copper

(Cu) substrate, epitaxial growth by thermal deposition of Si atom from the SiC surface and colloidal suspension from graphite oxidant have been developed [20].

## **2.2. Properties of Graphene**

Graphene occurs waves on the surface due to its properties and honeycomb network structure. The waves generated on this surface can stimulate the local electrical and optical properties of graphene [21]. The remarkable properties of graphene include quantum hall effect at room temperature, ambipolar electric field effect and ballistic transfer of load carriers, adjustable bandwidth and high flexibility. While graphene is expected to be completely flat, fluctuations are caused by thermal fluctuations. Ideally, graphene is a single-layer material, but two or more layers of graphene samples are examined with equal interest [17].

### **2.2.1. Electrical Properties**

The graphene revolution began with an examination of the electrical and electronic properties of graphene. These properties depend largely on the number of graphene layers on the graphene sheets. Novoselov et al. on the graphene, the potential charge in the transistors showed due to the possibility of charge carriers ranging from holes to electrons [5]. This electron hole dependence can only be applied to single-layer graphene sheets, but if the number of layers starts to increase, the dependence is weakened due to the electrical field scanning of other fields [10].

It has been found that the quantum Hall effect of graphene for both electron and hole carriers is due to the extremely high electron mobility of graphene under exposure to various temperatures and magnetic fields. At room temperature, this may exceed  $2000 \text{ cm}^2 \text{ V}^{-1}\text{s}^{-1}$  for mechanically produced graphene [21]. Typically, the classical integer quantum Hall effect, the electron charge  $e$  and  $h$ , occurs at Planck's constant  $4e^2/h$ , but in graphene, it occurs only at half integers. This effect is believed to result from the unique

graphene band structure. The electron mobility of graphene depends on the temperature and substrate used [15].

### 2.2.2. Mechanical Properties of Graphene

Carbon-based materials naturally exhibit excellent mechanical properties. For example, diamond is known as hardest naturally-occurring material, and carbon nanotubes are with their highest tensile strength. Graphene is not different in its extreme mechanical properties. Lee et al. [8]. They also showed that single-layer graphene had more than 200 times the breaking strength of steel and Young had 1 TPa modulus [8]. However, it is believed that these values depend on the purity of the graphene layers. Frank et al. I measured Young's AFM monolayer graphene module at 0.5 TPa. Dikin et al. graphene oxide paper showing elastic modulus of about 32 GPa and fracture strength of about 120 MPa. To improve the mechanical properties of these graphene papers, divalent ions and polyallylamine were introduced between the layers by chemical crosslinking. A summary of some of the mechanical properties of graphene is presented in Table 2.1. It is clear that the thickness of the graphene layers has a large effect on the properties [21].

Table 2.1. Table of results obtained using AFM of mechanical properties of graphene [8].

Graphene layers	Mechanical properties	
	Young's modulus, E (TPa)	Intrinsic strength, $\sigma$ (GPa)
One	1	130
One	1	131
Two	1.04	125
Three	0.98	101

### 2.2.3. Optical Properties

Although only one atom thick, graphene can absorb 2.3% of white light. Two-layer graphene absorbs up to 4.6% of white light [5]. Basically, it was found that the absorption of white light increased almost linearly with the increase in graphene layers, each layer absorption  $A = 1 - T = \pi\alpha = 2.3\%$ , where  $\alpha \sim 1/37$  is the fine structure constant [15]. Graphene can also be identified by optical microscopy on a Si/SiO<sub>2</sub> substrate due to interference. In the UV region, between 900 and 300 nm, the absorption spectrum of graphene is non-specific and it can be seen that the maximum absorption peak is at about 270 nm [21].

### 2.2.4. Thermal Properties

The thermal conductivity of graphene is dominated by phonon transport, i.e. diffusive and ballistic conductivity at high and low temperatures. However, due to the low carrier density of the non-doped graphene, electronic thermal transport within the graphene can be omitted [21]. The internal thermal conductivity of graphene is about 2000-6000 Wm<sup>-1</sup> K<sup>-1</sup> for suspended graphene sheets at room temperature and  $\sim 600$  Wm<sup>-1</sup> K<sup>-1</sup> for suspended graphene in SiO<sub>2</sub> substrate [5]. These values are highly dependent on graphene defects such as edge scattering, isotopic doping and sample production residues, which cause background scattering and localization. Therefore, high thermal conductivity values are obtained with the graphene produced by the MC method due to the high quality of the sheets [11].

### 2.2.5. Chemical Properties of Graphene

Pure graphene sheets are mostly non-reactive. Functionalization of the surface is necessary to reactivate it with other materials. Graphene sheet chemical is dominated by

its surface and graphene nanoribbons at its edges [5,15]. Thickness also plays a very important role in graphene reactivity. For example, the relative irregularity (D) peak in Raman spectroscopy was determined by Sharma et al. To be nearly 10-fold more reactive than monolayer graphene bi or multilayer graphene. Using spectroscopic testing, they compared the reactivity of the graphene edges with the bulk materials. The reactivity of the edges was found to be at least twice higher than the reactivity of the bulk single graphene sheet [15,21]. One way of functionalizing the graphene layers is by means of nitrenic chemistry, i.e. hydroxyl, bromine, carboxyl, amino, and the like. Such is the introduction of reactive species covalently bonded to the surface of graphene. Different solvents. These sheets can be easily processed and used in a variety of applications such as nano-hybrids and for the manufacture of polymer composites [4].

### **2.3. Graphene Based Biosensors Applications**

Graphene and its derivatives have been the preferred nanomaterials in many biosensor studies, including electrochemical biosensors, electrochemiluminescent (ECL) biosensors, and FET biosensors [83,85].

Among the nanomaterials used for biosensor production, graphene and graphene based nanomaterials are used in biosensor studies more than other materials because they provide an improved signal response in various detection applications [82]. Furthermore, graphene-based nanomaterials have high surface area, and because graphene and its derivatives are carbon-based nanomaterials, they offer excellent biocompatibility with various biomolecules such as antibodies, enzymes, DNA, cells and proteins. The inclusion of such biological molecules in the detection scheme of graphene has allowed the development of graphene-based biosensors [85]. Graphene-based biosensors can detect multiple molecules, biomolecules, and even cells. Figure 2.4 shows the parts that must be present in a biosensor and the components that interact with the graphene surface.

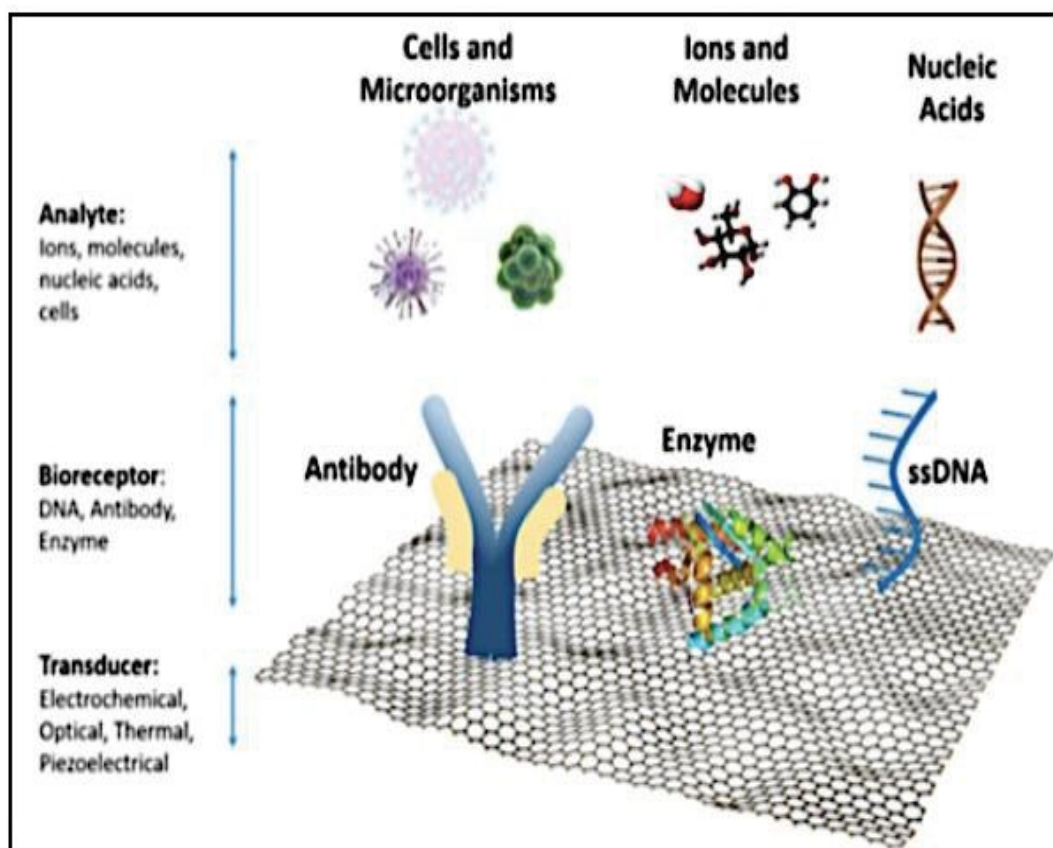


Figure 2.4. Schematic representation of a graphene platform and biosensor components [90].

In general, sensors consist of two elements, defined as a receptor and a transformer. The receptor is an organic or inorganic material that specifically interacts with the target molecule. The target molecule may be organic, inorganic, living cells or pathogens [82,83]. The transducer is the part of the biosensor that can measure its chemical data and convert it into a signal. Graphene-based nanomaterials are used as transducers of biosensors involved in converting interactions between receptor and target molecules into detectable measurements [83]. To obtain detectable data from these measurements, it is necessary to functionalize the bioreceptor molecules (such as antibodies, ssDNA and enzymes) on the transducer surface. The most common bioconjugation method for immobilization of antibodies and ssDNA on graphene and derivatives (graphene oxide, reduced graphene oxide) is EDC / NHS chemistry, while enzymes are most commonly immobilized using physisorption [81,89]. The most common attachment methods such as EDC / NHS chemistry and physisorption of bioreceptors show in Figure 2.5.

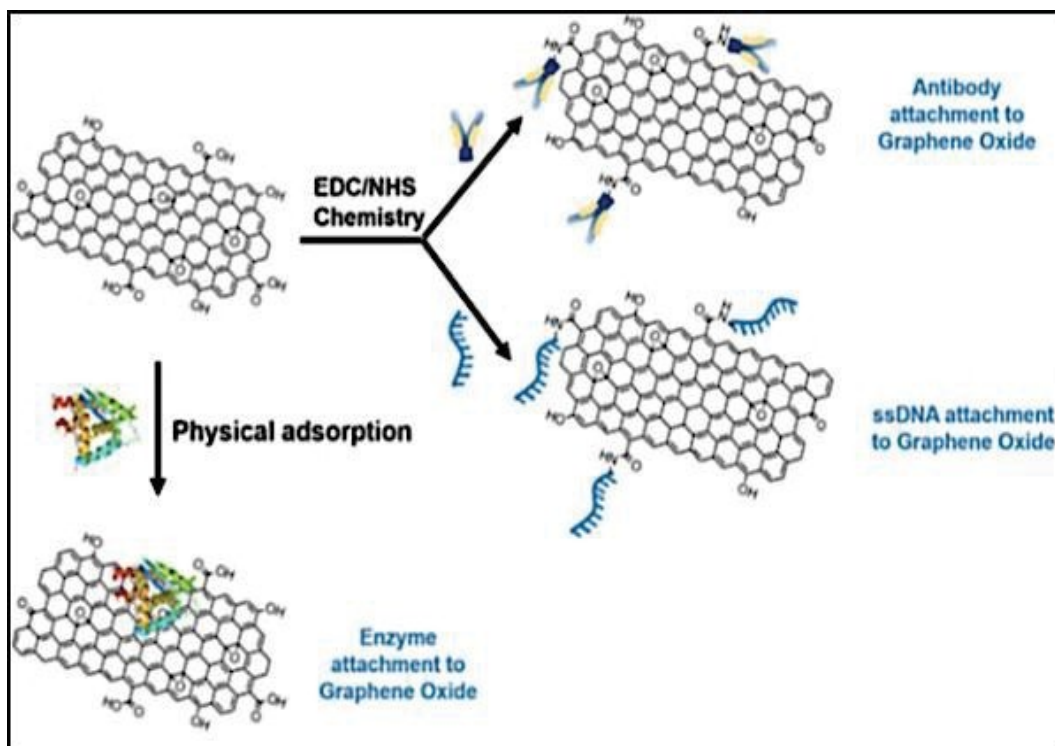


Figure 2.5. Representation of the most common attachment methods of bioreceptors [90].

Graphene has been used in the design of different biosensors of various transduction modes due to its large surface area, electrical conductivity, high electron transfer rate and the ability to immobilize different molecules. For example, the conjugate structure of graphene can facilitate electron transfer between the bioreceptor and transducer, which can produce high signal sensitivity for electrochemical sensors. Furthermore, the graphene-based nanomaterial can act as a quencher in the transducer to produce fluorescent biosensors. Studies have shown that graphene (G), graphene oxide (GO) and reduced graphene oxide (rGO) have a very high fluorescence quenching efficiency [84].

Different synthetic batches of graphene and derivatives and different synthetic methods can lead to different properties and functions of graphene-based nanomaterials in biosensors. The orientation between the G, GO or rGO sheets and the bioreceptor can also directly affect the selectivity and sensitivity of the biosensors. In addition, the number of layers, functional groups, and oxidation states of graphene and derivatives will cause differences in the detection performance between the sensors and even affect the bond between the transducer and the bioreceptor. The amount of functional groups in the nanomaterials can also affect the interactions and limit of detection of the target molecule [87,88].

The "body" of the Ab fragment consists of two different fragments, the crystallizable fragment (Fc) and the antigen binding fragment (Fab). Fc and Fab contain carboxyl ( $-\text{COOH}$ ) and amino ( $-\text{NH}_2$ ) groups that bind to the target molecule with high affinity. This high affinity recognition against a specific antibody-antigen reaction is mainly due to the structure, properties and reactivity of the antibodies, making them excellent for detection applications [86].

The versatility of the functional groups of the GO surface allows different strategies for Ab binding. Most strategies for functionalizing GO with antibodies include 1-ethyl-3-(3-dimethylaminopropyl) carbodiimide hydrochloride (EDC) / N-hydroxysuccinimide (NHS) (EDC / NHS) chemistry reaction with electrostatic coupling or pyrene derivatives.

Functionality through EDC / NHS chemistry is the most popular and versatile method for producing biochemical conjugations. EDC is a water-soluble cross-linking agent that allows direct bioconjugation between carboxyl and amine groups. In this reaction, the nucleophilic attack from the primary amine group from the antibody forms an amide bond with carboxyl groups on the surface GO. This process may form conjugates between two different molecules with an amide group [81,89].

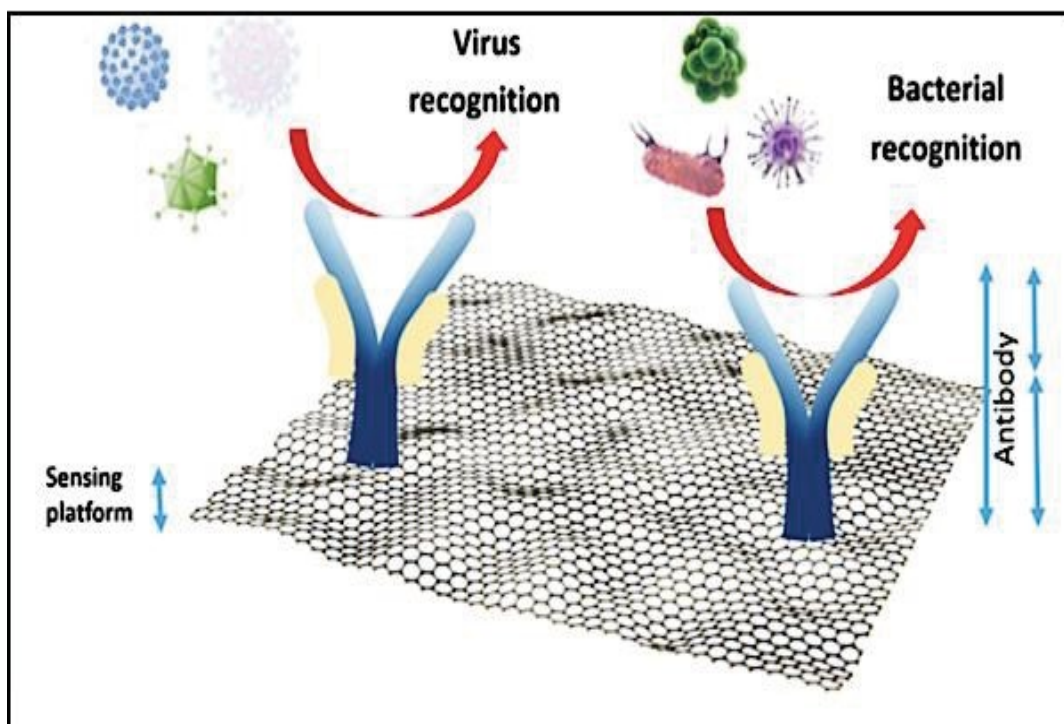


Figure 2.6. Schematic representation of graphene surface modified with antibodies for the recognition of pathogens [89].

There are two main types of sensors in DNA biosensors that use graphene-based nanomaterials as transducers: electrochemical and fluorescent sensors. The electrochemical sensor is based on measurements of the changes in voltage, current or impedance that may result from changes in electrochemical factors, such as electron loss, conductivity or capacitance changes, which are caused by the hybridization of DNA or the oxidation of adenine (A), thymine (T), cytosine (C) and guanine (G) of the DNA [80].

The electrochemical signals generated by these biosensors can be detected using cyclic voltammetry (CV), differential pulse voltammetry (DPV), or electrochemical impedance spectroscopy (EIS). In the electrochemistry approach, immobilization of DNA is done by  $\pi$  -  $\pi$  interactions on the surface of graphene-based nanomaterials. G edges and GO or rGO with their functional groups (carboxylic, hydroxyl and epoxide groups) can also be used to covalently interact with the DNA.

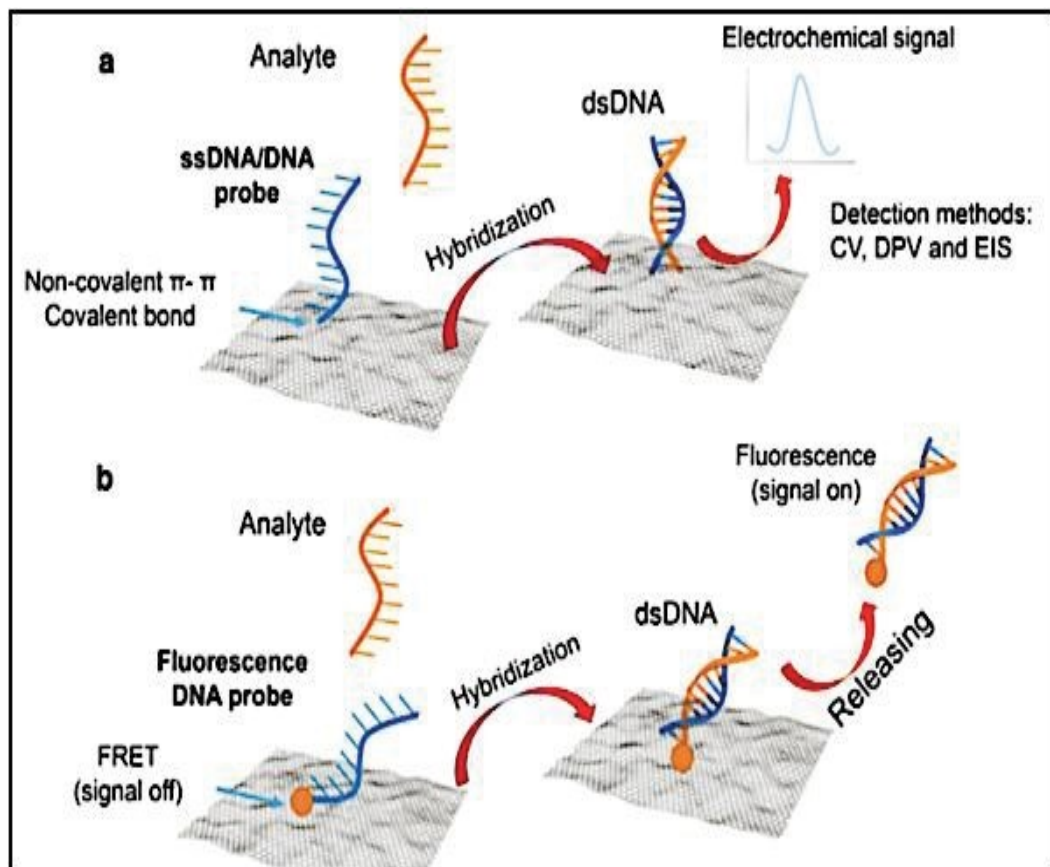


Figure 2.7. Schematic representation of graphene-based nanomaterials as a DNA biosensor Electrochemical detection (a) and fluorescence detection (b) [80].

The fluorescent DNA nanobiosensor is based on hybridization of two single-stranded DNA (ssDNA). One ssDNA is labeled with a fluorescent dye and the other is

complementary DNA corresponding to the target DNA. This method requires optical detection; therefore, it utilizes the optical quenching property of graphene-based materials to enhance visualization and detection of the target ssDNA. The immobilization of the fluorescent-labeled DNA can be carried out by direct adsorption of the DNA probe on the graphene-based surface through the  $\pi$ - $\pi$  interaction between the ring structure of the DNA bases and the graphene surface [79,80].

The two methods seem to be effective and offer low detection limits. However, each technique has advantages and disadvantages which depend on the ability to immobilize DNA and the method of measurement in substantially graphene-based nanomaterials. Electrochemical detection method takes into account the large surface area and conductivity of nanomaterials. The detection is based on the base types and numbers present in the DNA that will cause changes in the electrical potential for measurement. Therefore, homogeneous deposition of the probe on the graphene material is essential for accurate measurements. In addition, electrostatic potential and DNA length can affect the efficiency of the sensor. On the other hand, fluorescence detection can be performed in ssDNA or dsDNA regardless of the length of the DNA. This method is based on the extinguishing and optical capabilities of graphene-based nanomaterials. One of the main disadvantages of this method is that it can overestimate the fluorescence signal in some complex samples such as serum samples due to the high background fluorescence signal. On the other hand, the fluorescently labeled probe may lose its intensity (photo-bleach) over time [84].

## **2.4. Functionalization Strategies of Graphene Surface**

Essentially there are three approaches for functionalization of the graphene surfaces to control its chemical properties; (i) Non-covalent modification through weak interactions, (ii) intercalation of molecules between graphene sheets and underlying substrate and (iii) covalent modifications of the graphene lattice [49]. Non-covalent and covalent modification of the graphene surfaces are more preferred methods in biological applications (Figures 2.7 and 2.8). The functionalization of the graphene surface is necessary to ensure the interaction of biological molecules with the surface [49,52].

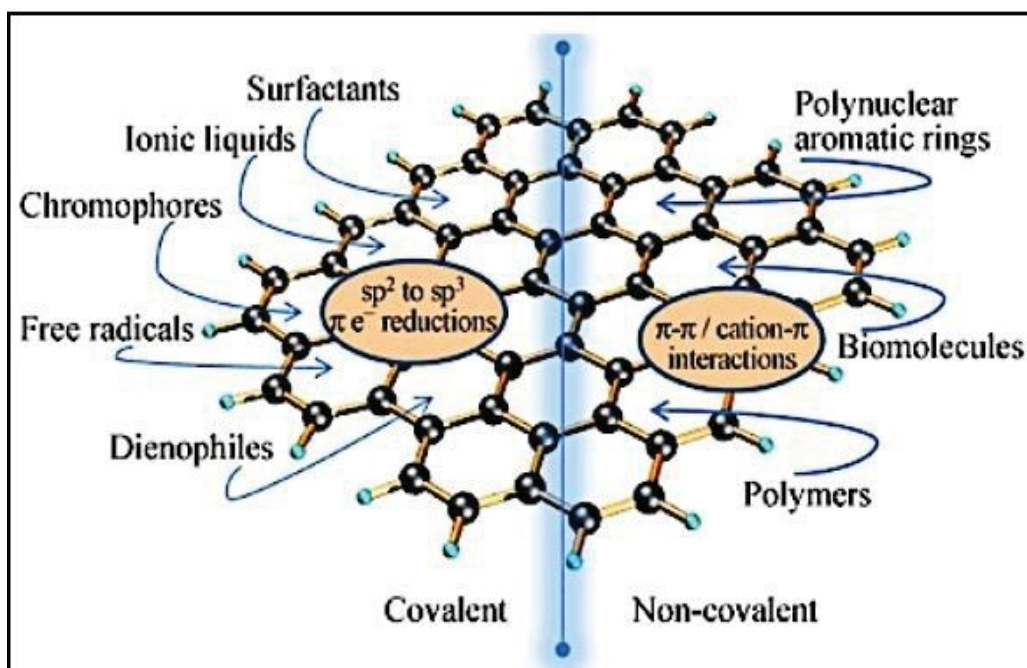


Figure 2.8. Schematic representation of the covalent and non-covalent functionalization of graphene [60].

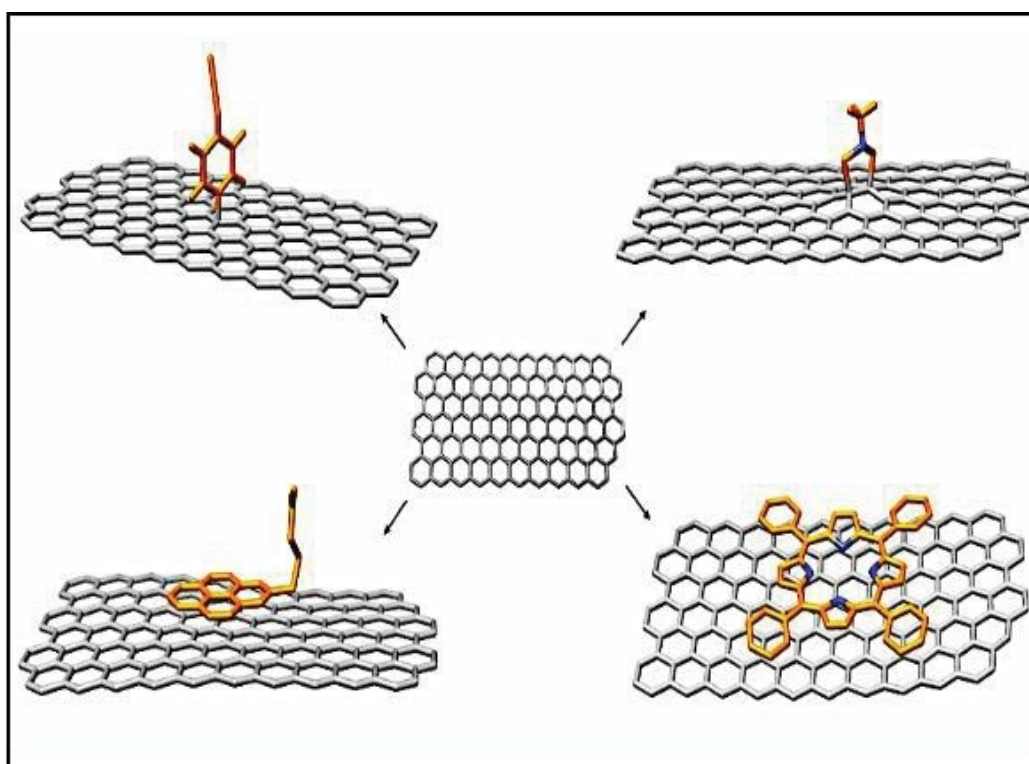


Figure 2.9. Schematic demonstration of the covalent (up) and non-covalent (down) functionalization of graphene [49,53].

## 2.4.1. Covalent Functionalization of Graphene

The covalent addition of different functionalities to the graphene surfaces occurs via oxygen bonds, often referred to as "oxygenated functional groups" or structural  $\pi$ - $\pi$  networks [49]. Furthermore, the presence of carboxylic acid groups at the edges and epoxy / hydroxyl groups on the basal plane of graphene and graphene oxide is used to adapt the surface functionality of the graphene surfaces [50].

Covalent modification of graphene with various organic functionalities has been done using two general pathways: (1) combining free intact graphene C - C bonds with radicals or dienophils; and (2) reacting the oxygen groups of GO with organic functional groups. Based on previous studies on fullerene and carbon nanotubes, the most attractive organic species for reaction with  $sp^2$  carbons in graphene are organic free radicals and dienophils. Generally, both of these species are intermediate reactive components produced under certain conditions in the presence of graphene [49,51].

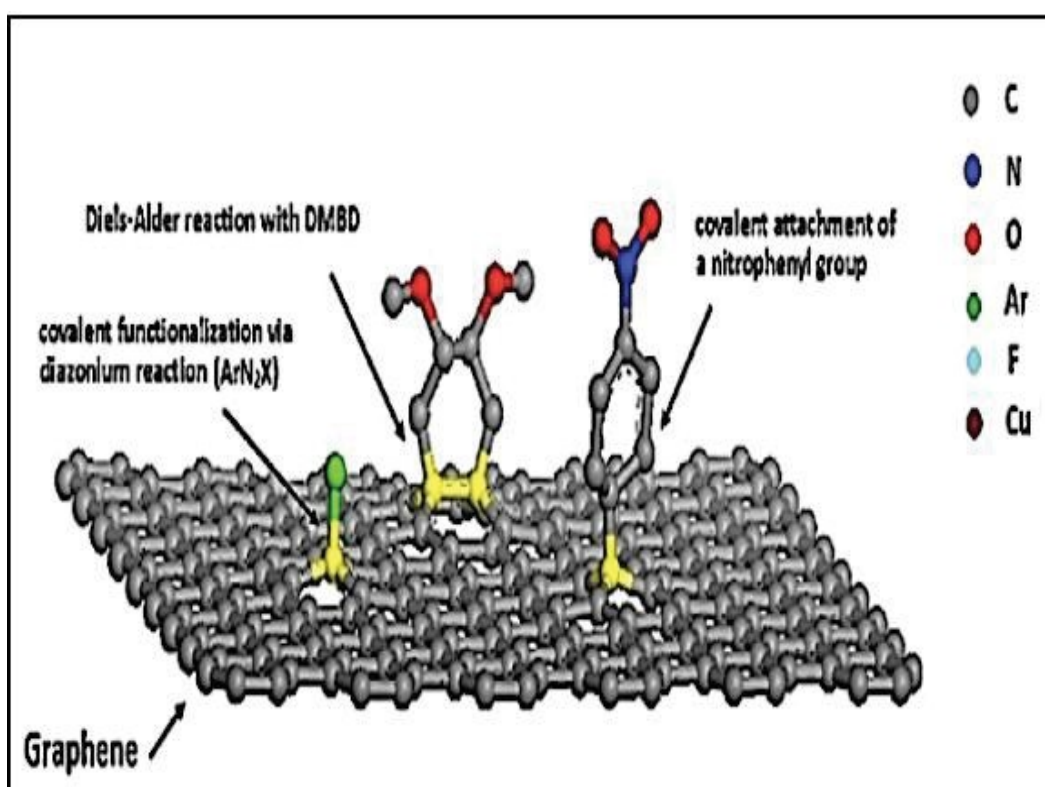


Figure 2.10. Representation of covalent modification of graphene surface with Diels Alder Reaction [49].

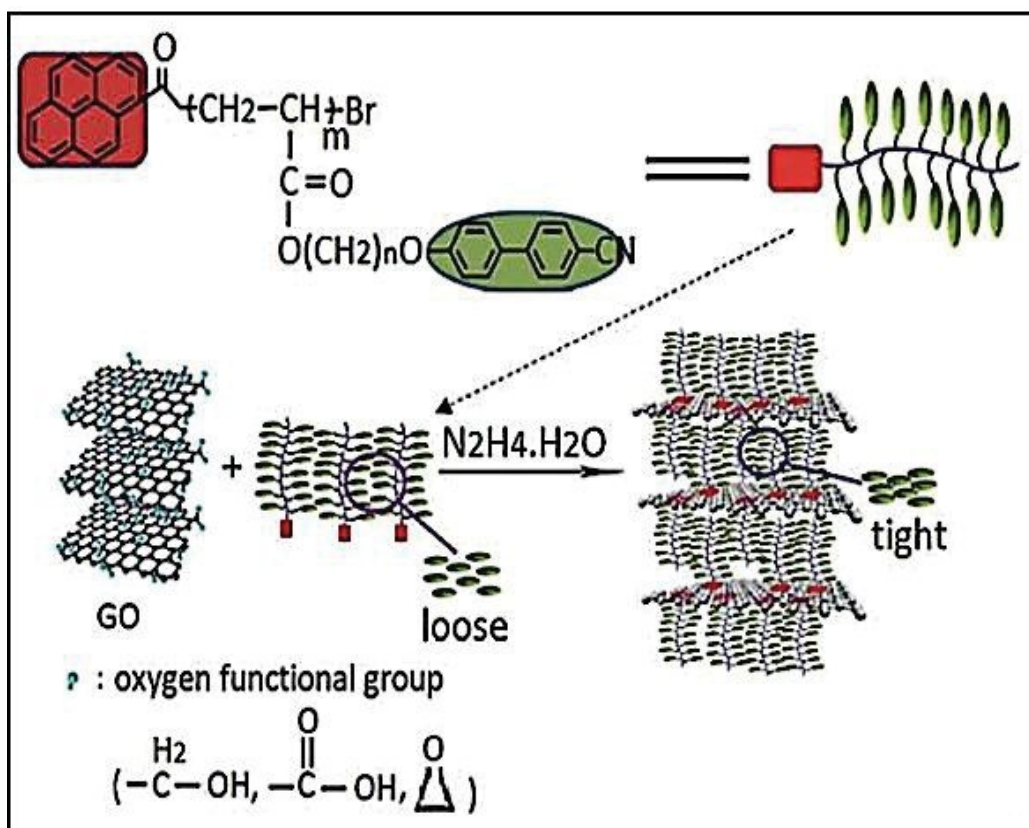


Figure 2.11. Representation of covalent modification of graphene surface with organic cross-linkers [52].

## 2.4.2. Non-Covalent Functionalization of Graphene

Any distortion of the structure of the basal graphene plane refers to altering the properties that make it a superior material. This involves covalent functionality, since the formation of new bonds changes the hybridization of carbon atoms from  $sp^2$  to  $sp^3$ . Non-covalent functionality is a physical process that takes advantage of the adsorption of molecules to the graphene surface and allows the preservation of its own skeleton and its associated properties [56].

$\pi$ - $\pi$  interactions define dominant non-covalent forces in  $\pi$  systems and the functionalized structure of graphene. Therefore, in the non-covalent functionalization studies of graphene, planar aromatic molecules and derivatives thereof are preferred. It is known that pyrene and its derivatives show strong tendencies towards the graphene basal plane in non-covalent functionalization studies (Figure 2.12) [60].

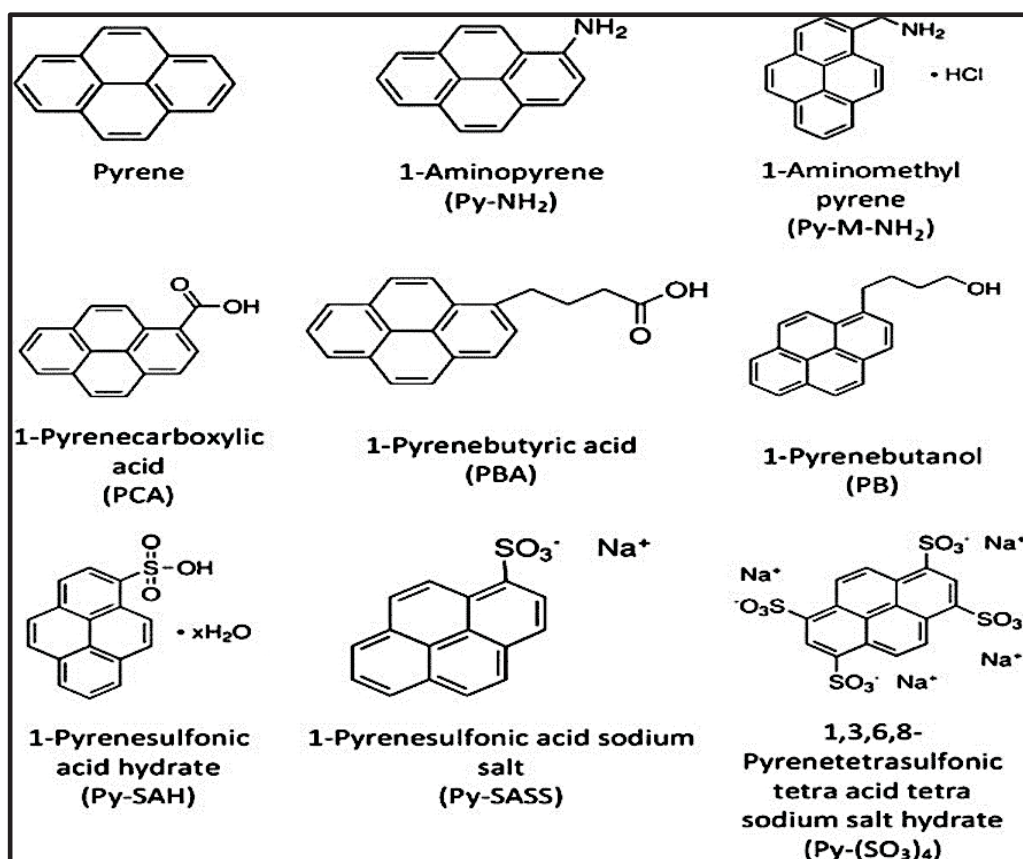


Figure 2.12. Schematic representation of pyrene derivatives used for non-covalently functionalization of graphene [57].

The use of pyrene butyric acid provides stable and robust functionalization by stacking four aromatic rings, while the terminal acid function remains free and usable for further covalent inoculation of biomolecules with amine functions [53,57].

## 2.5. Antibody-Cell Receptor Interaction

Antibodies are protein-based biomolecules secreted by B cells in the bone marrow and having a Y-shaped structure [62]. Furthermore, an antibody molecule has two heavy chains (H) and two light chains (L) in the structure. These chains contain NH<sub>2</sub> at one end and COOH molecules at the other end. The NH<sub>2</sub> end of the antibody molecule is called the aminothermal end and the COOH end is called the carboxyterminal end. The two arms of the Y shape vary between different antibody molecules in the V (Variable) regions [62,63]. They play a role in antigen binding, whereas the body of the C (Constant)

region is responsible for interacting with effector cells and molecules. The structure of the antibody molecules is shown in Figure 2.13. One of the major duties of antibodies is to provide an immune response to antigens such as bacteria, viruses and pathogens. In this way, antibodies play an important role in protecting our immune system against infections and diseases [68].

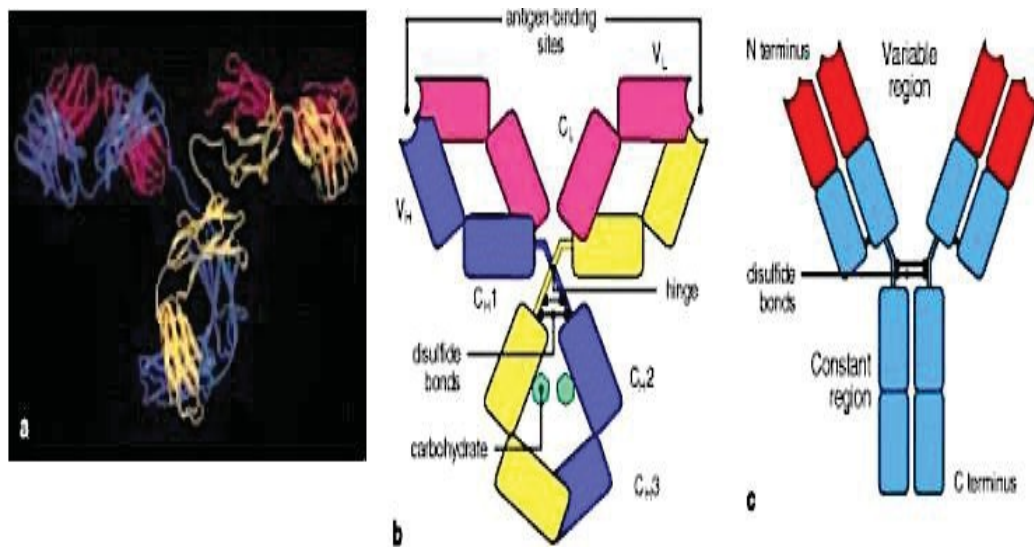


Figure 2.13. Schematic representation of antibody structure. (A) Schematic representation of the X-ray crystallographic structure of an IgG antibody. (B) Schematic representation of the four-chain composition of the antibody structure and the domains containing each chain. (C) representation of a simplified form of an antibody molecule [65].

Antibodies include small proteins of the immunoglobulin family (Ig) consisting of anti-parallel  $\beta$  layers [67]. Ig consists of two light chains with a molecular weight of 25 kDa and two heavy chains of 50 kDa forming the Y-shape of antibody molecules. These heavy and light chains are divided into two. The first is the N-terminus that forms part c that determines the antigen binding site and isotype [64,69]. Furthermore, the light chain and the heavy chain are comprised of two groups of Ig and four Ig domains, respectively. Depending on the antibody isotype [70,71] light chains and heavy chains are linked together by non-covalent and disulfide bond interactions [72]. The V chain and the heavy chain of the light chain are linked to form two antigen binding sites to enable the antibody to bind strongly to the antigen. When the V<sub>H</sub> and V<sub>L</sub> domains bind to the antibody, the hypervariable rings in these domains come together to form complementarity determining regions (CDR1, CDR2, and CDR3), ie the antigen binding region [74]. This CDR region consists of a combination of heavy and light chains and

defines the specificity of the antigen. Further, three CDR regions come together to form the surface of the antibody [75].

## CHAPTER 3

### MATERIALS AND METHODS

#### 3.1. Materials

4-(1-Pyrenyl)-butyric acid (PBA, 97.0%) was used as linker in graphene surface functionalization and purchased from Merck.

Methanol (Merck, high purity), ethanol (Merck, high purity), N,N-dimethylformamide (Merck, high purity), acetone (Tekkim, 99.5%), ethanol (Tekkim,96%), were used for graphene surface modification.

N-ethyl-N'-(3-dimethylaminopropyl)carbodiimide hydrochloride (EDC) was purchased from Merck. N-hydroxysulfosuccinimide (Sulfo-NHS) was purchased from Thermo Fisher Scientific.

Antihuman/NP CD2 (30 µg/ml) antibody was purchased from Invitrogen. 2-(N-Morpholino) ethanesulfonic acid hydrate (MES > 99.5) and sodium hydroxide (NaOH) were purchased from Sigma Aldrich. The mouse anti-Syndecan-1 [B-A38] monoclonal antibody used as a different antibody.

RPMI 1640 (+L-Glutamine, Gibco), fetal bovine serum (FBS, Gibco), penicillin- streptomycin (Pen-Strep, Gibco), phosphate buffer salt (PBS, 10X, Gibco), trypan blue (Biological Industries) were used for cell culture experiments. All chemicals were used as received.

Jurkat cells (T lymphocyte cell line) were donated by Prof. Dr. Yusuf Baran (İzmir Institute of Technology). Graphene surfaces were provided by Assoc. Prof. Dr. Cem Çelebi (İzmir Institute of Technology).

## **3.2. Instruments**

### **3.2.1. Raman Spectroscopy**

Raman measurements in this study were performed using XploRA PLUS system developed by HORIBA Jobin Yvon. In the measurements, solid state laser source emitting at 532 nm and diode laser at 785 nm were used as excitation sources. The optical imaging system integrated into the system is Olympus BX41 and the lenses with 10X, 20X, 40X and 100X magnifications of the same company were examined. The data acquisition time for each measurement was set to 10 s and each measurement was repeated 10 times. The spectra collected were normalized with the HORIBA data acquisition program LabSpec 6. For reproducibility and reliability of the measurements, Raman experiments were performed in 3 replicates.

### **3.2.2. X-Ray Photoelectron Spectroscopy (XPS)**

Elemental analyzes and structures of the samples were performed by Thermo Scientific K-Alpha Surface Analysis model X-ray photoelectron spectroscopy device. Measurements were taken from an area of 400  $\mu\text{m}$  diameter with X-rays produced by the alpha ray source. All graphene surfaces prepared were sent to XPS analysis with double control.

### **3.2.3. Stereo Microscope**

Stereo microscope was used to examine the surface of visible objects and provides a 3-dimensional image unlike light microscope. It was provided by Optical

Characterization Laboratory of Physics Department of Izmir Institute of Technology. Stereo microscope measurements in this study were performed using NIKON Photonic PL2000.

### **3.3. Methods**

#### **3.3.1. Functionalization of Graphene Surfaces**

Graphene surfaces were supplied from the Physics Department of the Izmir Institute of Technology. For functionalization of graphene surfaces, 4- (1-Pyrenyl)-Butyric acid (PBA) was dissolved at 10 mM concentration value in different solvents (methanol, ethanol, dimethylformaldehyde (DMF), ethanol and dmf mixtures (in different ratios), methanol and dmf mixture (different ratios) (24 hours). Graphene surface was placed into the prepared solution and allowed to incubate for 24 hours. Following incubation time, the surfaces were washed with the corresponding solvent system for several times. The binding of PBA to graphene surface was analyzed by both Raman spectroscopy and X-ray Photoelectron spectroscopy (XPS).

#### **3.3.2. Conjugation of Antibodies to Graphene Surfaces**

For antibody binding, PBA-modified graphene surfaces were first incubated for 10 minutes with EDC/NHS (EDC concentration: 15 mM and the NHS concentration was calculated such that the final concentration of the EDC/NHS solution was 5 mM) in MES buffer medium (pH 6). The graphene surfaces were then reacted in PBS (pH 7.2) with the anti-human CD2 antibody (0.1  $\mu\text{g}/\mu\text{l}$ ) for 6 hours at room temperature. Following the incubation time, the surfaces were washed with PBS for several times and then characterized via Raman spectroscopy and XPS.

### **3.3.3. Interaction of Antibody-Functionalized Graphene Surfaces with Cells**

The Ab-conjugated graphene surfaces were immediately used for interaction with Jurkat cells. After the results obtained from the experiments and determination of certain parameters, graphene surface and cell (Jurkat cell line) interaction experiments were started.

Two different methods were used for the interaction of Ab-functionalized graphene surfaces with Jurkat cells: Firstly, the surfaces were incubated in the cell suspension for 1 hour in different media (cell culture medium or PBS) at 4°C or 37°C. At the end of the incubation, the surfaces were removed from the suspension and the surface that removed were washed with PBS solution for several times. After washing, surface was analyzed. As a second method, the cell suspension in media or PBS was dropped onto the surfaces and incubated for 1 hour at 4°C or 37°C. After incubation, excess liquid was removed from the surface and analyzed by adding fresh (cell-free) medium or PBS. Non-functionalized surfaces with the antibody as the control assay were subjected to the same treatments and analyzed.

### **3.3.4. Cell Culture**

Jurkat cells (human T lymphocyte cell line) were grown in RPMI 1640 culture containing 10% FBS and 1% penicillin / streptomycin in an atmosphere of 5% CO<sub>2</sub> at 37 °C. When the cells reached 80% fullness, the cells were passaged by centrifugation at 800 rpm for 5 minutes. In the next step after centrifugation, the medium was gently withdrawn by pipette and the cells were resuspended by pipetting in new medium.

## CHAPTER 4

### RESULTS AND DISCUSSION

#### 4.1. Functionalization of Graphene Surfaces

To develop graphene-based biosensors, functionalization of graphene is required for enabling covalent conjugation of biomolecules such as antibodies. Pyrene butyric acid (PBA) has been widely used in the literature for functionalization of graphene [76]. Graphene and PBA stably interacts through hydrophobic and pi-pi interactions [76, 77]. There is a number of experimental methods reported in the literature for functionalization of graphene with PBA. A number of different solvents such as ethanol, methanol, dimethylformamide, chloroform has been used for interacting graphene with PBA in the literature. In this study, the most suitable solvent for PBA-graphene interaction was firstly investigated. Solvents with varying polarity index values (Table 4.1) were chosen to be tested.

Table 4.1. Polarity index values of solvent systems tested for graphene-PBA interactions.

Solvent Name	Polarity Index Value, P
Ethanol	5,2
Dimethylformamide	6,4
Methanol	6.6

Graphene surfaces were incubated with PBA (10 mM) in different solvents as indicated in Table 4.1 and washed with the same solvent system for several times before analyzing via Raman Spectroscopy. The Raman spectra of the samples are presented in Figure 4.1.

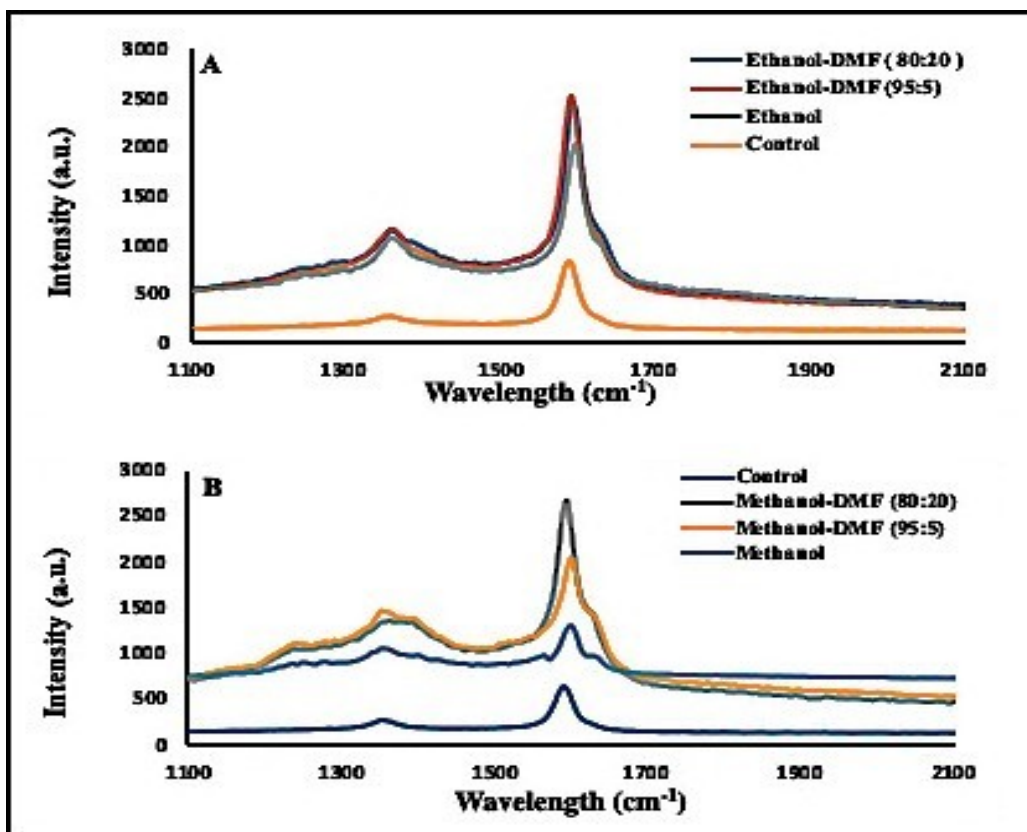


Figure 4.1. Raman spectra of graphene surfaces after functionalization with PBA (10 mM) in different solvents (A) Ethanol and mixtures with DMF at different v:v ratios (B) Methanol and mixtures with DMF at different v:v ratios

In the RAMAN spectra, graphene displayed 4 peaks in the range between 3100 and 1100  $\text{cm}^{-1}$ . These peaks are as follows; peak at around 1360  $\text{cm}^{-1}$  due to its corresponds to disordered carbon structure, peak at 1590  $\text{cm}^{-1}$  due to corresponds to  $\text{sp}^2$  carbon systems and C-C bond because of graphitic structure, peak at 2350  $\text{cm}^{-1}$  due to observed defects or impurities.and peak at around 2680  $\text{cm}^{-1}$  due to  $\text{sp}^2$  carbon systems . The peak at around 2680  $\text{cm}^{-1}$  depends on the number of layer graphite structure. Also, the ratio of peak at around 2680  $\text{cm}^{-1}$  and peak at 1590  $\text{cm}^{-1}$  gives significant information about the number of layer graphitic carbon. When the graphene surface was modified with PBA, deformations were observed at 2350  $\text{cm}^{-1}$ . Moreover, a new signal at 1650  $\text{cm}^{-1}$  appeared which was attributed to  $\text{sp}^2$  -  $\text{sp}^2$  hybridization of carbon atoms. These changes indicated that the graphene surface was functionalized with PBA. From the Raman spectra, functionalization of graphene with PBA appeared to be more clearly when Methanol and its DMF mixtures was used as solvent. Raman is a qualitative analysis method although raman microscopy also helps in understanding the graphene surface functionalization process. The studies were continued with XPS analysis which is a

quantitative analysis method since it does not show the bond structures directly. Surfaces treated with PBA in methanol or methanol: DMF mixtures were further analyzed by X-ray Photoelectron Spectroscopy (XPS). C1s XPS data are presented in Figure 4.2.

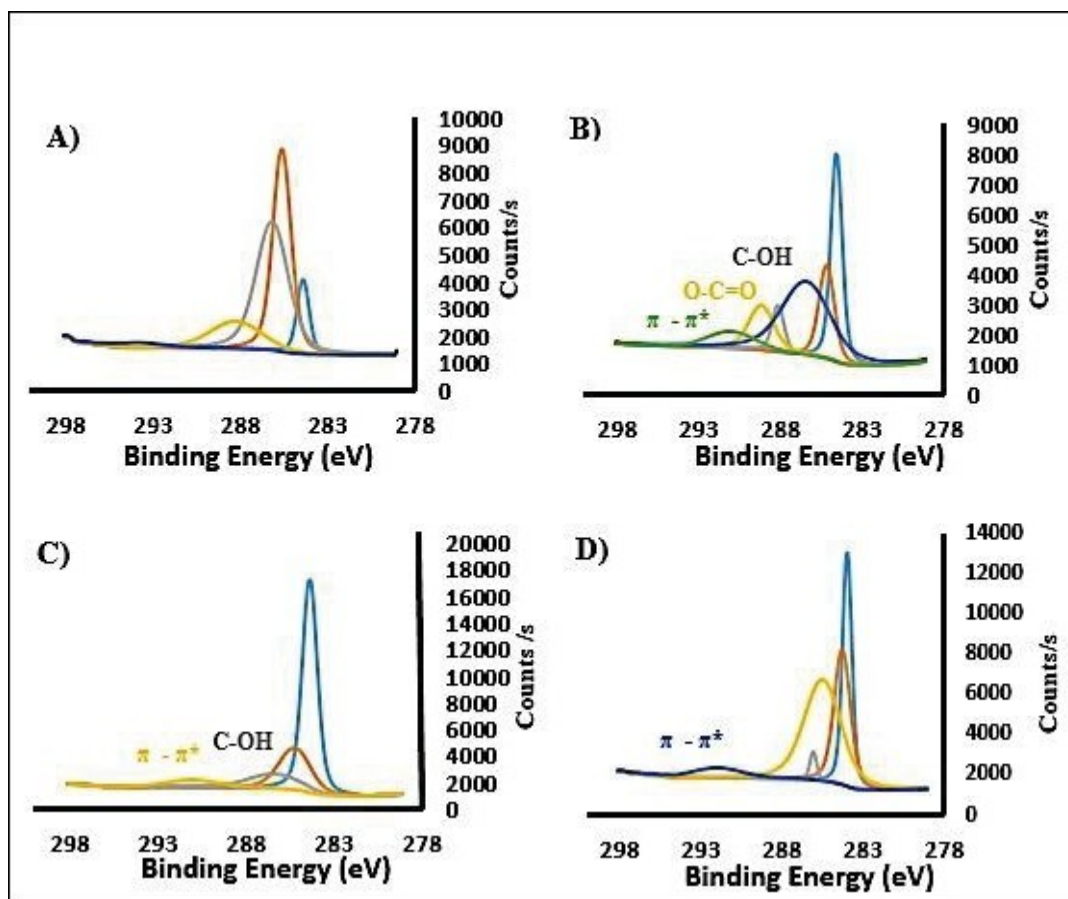


Figure 4.2. C1s XPS spectra of graphene surfaces (A) non-functionalized (B) after functionalization with PBA using methanol (C) after functionalization with PBA using methanol:DMF (80:20) (D) after functionalization with PBA using methanol : DMF (95: 5)

When the XPS results were evaluated, 5 distinct C1s bands for the non-functionalized graphene surface were observed in Figure 4.2A. The band at 284.54 eV was assigned to C-C  $sp^2$  hybrids, C = C and C-H bonds. The band at 285.14 eV corresponds to C-C  $sp^3$  hybrids. The bands at 288.13 eV and 289.15 eV correspond to C- O and C=O bonds which might be due to adventitious carbon contamination. Figure 4.2B shows the C1s XPS data of graphene surface functionalized with PBA in methanol. Unlike the non-functionalized graphene sample, new bands appeared at 286.41 eV corresponding to C-OH bond, 289.15 eV corresponding to O-C = O bond

and 291.03 eV corresponding to O-C = O bond along with  $\pi$ - $\pi^*$  interactions. The surfaces functionalized

in methanol: DMF mixtures showed similar bands at lower intensities attributed to the same chemical groups. The average atomic values of C1s and O1s obtained from graphene surfaces before and after modification with PBA in different solvents are presented in Table 4.2. Additionally, the average atomic values normalized according to the average atomic value of Si2p were presented in Table 4.3.

The normalized C1s and O1s atomic percentages were expected to increase after modification of graphene surfaces with PBA. As expected an increase in both normalized C1s and O1s percentages of the surfaces after functionalization indicated that the surfaces were functionalized with PBA in all three different solvent systems. When three different solvents were compared, when DMF content was increased C1s values were found to increase while O1s values decreased. Considering that carbon contamination might be causing this inconsistency, the solvent that yielded significant increase in both C1s and O1s percentages was chosen for functionalization of graphene in further experiments. According to this evaluation, methanol was found to be appropriate as the solvent in the functionalization of the graphene surfaces.

Table 4.2. The average atomic percentage values of the Si2p, C1s and O1s of the graphene surfaces before and functionalization with PBA in different solvents

<b>Average Atomic Percentage %</b>				
<b>Atomic Name</b>	<b>Graphene (Before functionalization)</b>	<b>GRP+PBA (after functionalization in Methanol)</b>	<b>GRP+PBA (after functionalization in Methanol:DMF of 95:5)</b>	<b>GRP+PBA+ (after functionalization in Methanol: DMF of 80:20)</b>
<b>Si2p</b>	19,0	13,6	11,7	11,5
<b>C1s</b>	46,5	53,8	59,5	62,2
<b>O1s</b>	29,0	34,6	22,9	19,9

Table 4.3. The average atomic percentage values of the C1s and O1s normalized to the average atomic percentage values of the Si2p of the graphene surfaces before and functionalization with PBA in different solvents

<b>Normalized Average Atomic Percentage %</b>				
<b>Atomic Name</b>	<b>Graphene</b>	<b>GRP+PBA+ Methanol</b>	<b>GRP+PBA+ Methanol-DMF (95:5)</b>	<b>GRP+PBA+ Methanol- DMF (80:20)</b>
<b>C1s</b>	2,5	4,0	5,1	5,4
<b>O1s</b>	1,5	2,5	2,0	1,7

## **4.2. Antibody Conjugation to Functionalized Graphene**

After the appropriate solvent was determined for the functionalization of the graphene surface, experiments were carried out to perform covalent conjugation of a specific antibody to functionalized graphene surfaces. AntiCD2 antibody specific to human T cell receptors on Jurkat cells was used for these experiments. Briefly, PBA-functionalized graphene surface was first treated with NHS/EDC to activate the carboxylic acid groups on the surface. The activated surface was then incubated with antibody solution in phosphate-buffered saline (PBS) for 6 h at below room temperature. At the end of incubation time, the surface was washed several times with PBS and then analyzed via XPS.

XPS was used to monitor the transformation of chemical content changes and surface chemicals by utilizing binding energies after functionalization of the graphene surface with various intermediate molecules and antibody.

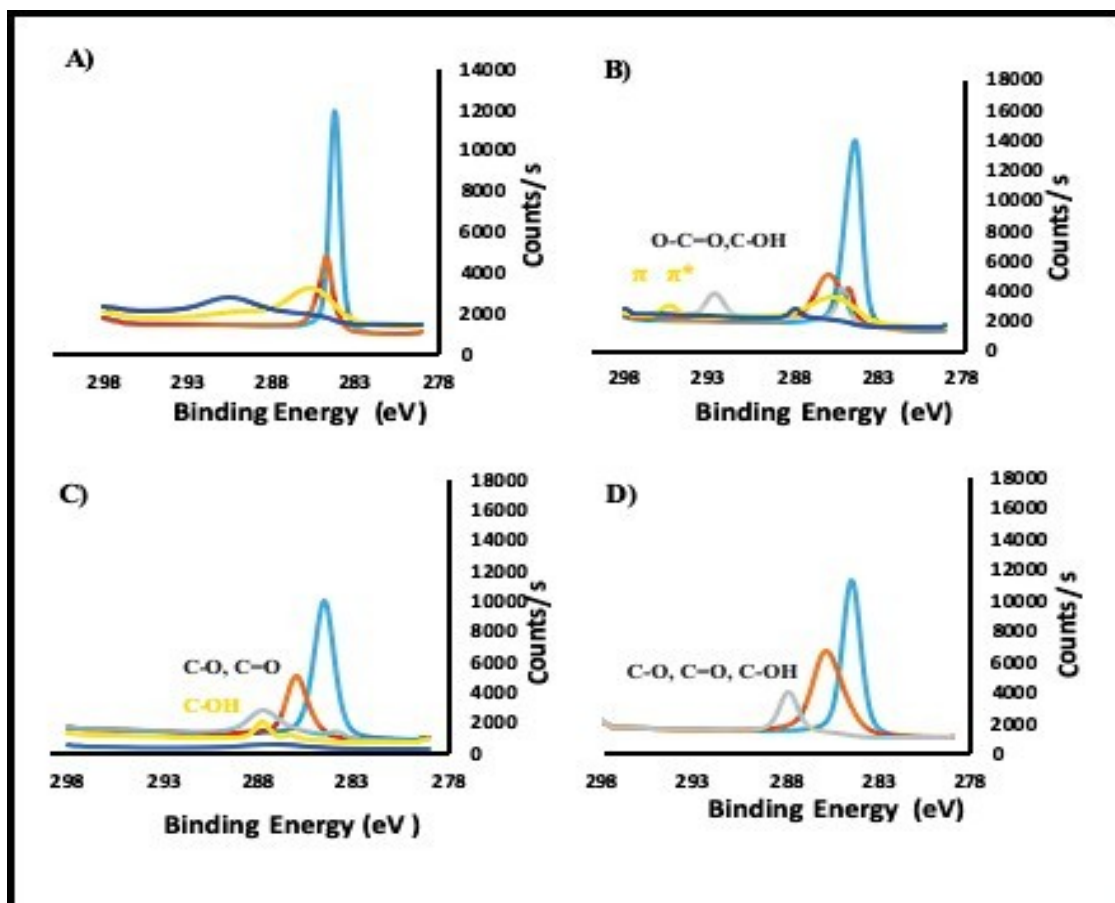


Figure 4.3. C1s XPS spectra of the functionalized graphene surface (A) Spectrum of the non-functionalized graphene surface (B) Spectrum of the PBA-functionalized surface (C) Spectrum of the PBA-functionalized surface activated with Ab directly (D) Spectrum of the antibody-conjugated graphene surface

Figure 4.3A and B show the C1s XPS data of the non-functionalized and PBA-functionalized graphene surfaces. Expected bands of graphene and PBA-functionalization were observed in accordance with Figure 4.3B Figure 4.3C shows the results of XPS measurement of PBA-functionalized graphene surface after conjugation with antibody (Ab). The band at 283,92 eV corresponds to C-Si bond, 285,76 eV to C-OH bond, 287,11 eV and 287,57 eV bands correspond to C-O, C = O and C-OH bonds. Figure 4.3D shows the results of XPS measurements after applying EDC / NHS chemistry to the PBA-functionalized graphene surface. When compared to the non-functionalized graphene sample, 285,80 eV corresponds to the C-OH bond and 287,94 eV corresponds to the C-O, C = O and C-OH bonds. In addition, the C atom percentage was found to increase in each step of the Ab conjugation procedure, as shown in Table 4.4. Importantly, N and O atoms were also significantly increased upon conjugation of

Ab to graphene surface. This directly indicates the successful conjugation of Ab molecules to PBA-

functionalized graphene surfaces. Additionally, N1s spectra were also evaluated to fully evaluate the success in Ab conjugation (Figure 4.4).

Table 4.4. The ratio of the average atomic percentage values of C1s, N1s and O1s atoms to the mean atomic percentage values of Si2p.

The ratio of C1s, N1s and O1s atomic percentage values to Si2p atomic percentage value			
Atom	GRP+PBA	GRP+PBA +Ab (control surface without treatment with EDC/NHS)	GRP+PBA+ED C/ NHS +Ab
C 1s	5,0	7,5	15,0
N 1s	0,2	0,9	1,7
O 1s	2,8	2,9	5,4

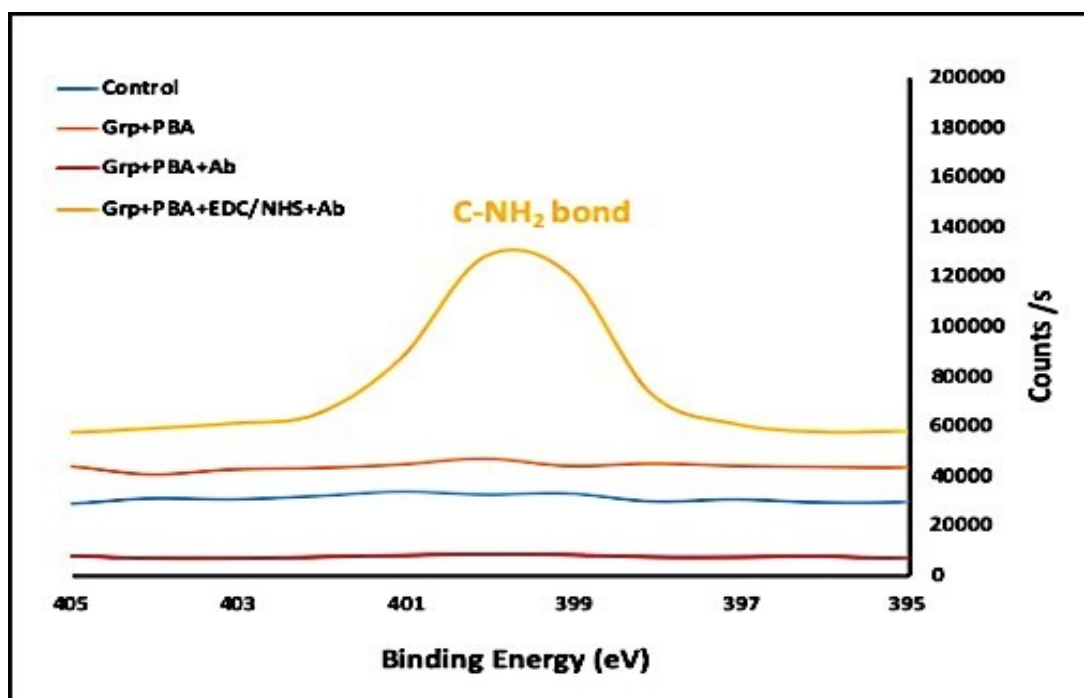


Figure 4.4. N1s XPS spectra of the functionalized graphene surfaces and non-functionalized graphene surface

Figure shows the N1s XPS scan of the PBA functionalized graphene surface. There is a single peak in N1s and the binding energy value at 400.09 eV was attributed to N-Si<sub>2</sub>-O group which might be due to contamination. After interaction with Ab in the presence or absence of NHS/EDC, a significant band at 399.73-399.77 eV appeared which corresponded to the C-NH<sub>2</sub> and N- (C = O) – bonds. The N-C = O bond represent the peptide bond that exist in the protein structure. C-NH<sub>2</sub> bond might be due to the side chain amino groups of lysine residues in the protein structure. Furthermore, the N atom percentage was found to increase after Ab treatment. While the N atom percentage normalized to Si atom of graphene surface is 0.20% before Ab treatment, this value increased to 0.90% and 1.70% after Ab treatment in the absence and presence of NHS and EDC, respectively. This proves that the graphene surface is functionalized with antibody molecules. While there was some degree of non-covalent binding probably through electrostatic and hydrophobic interactions, the Ab binding through covalent bonds (in the presence of NHS and EDC) was more significant as expected. Overall the XPS analysis proved that the PBA-functionalized surfaces were covalently conjugated with Ab molecules in a successful manner.

### **4.3. Recognition of Cells by Antibody Conjugated Graphene Surfaces**

At the next step, Jurkat cells were interacted with antiCD2 antibody-conjugated graphene surfaces. It was anticipated that Jurkat cells would bind to the antibody-functionalized surface because human T cell receptors specific to antiCD2 antibodies are present on Jurkat cell surface. A number of optimization experiments were performed to identify the best conditions for cell recognition. These experiments aimed to investigate the effect of temperature (4 °C vs 37 °C), interaction medium (PBS vs. cell culture medium), interaction method (dropping vs. dipping).

First, cells were incubated with Ab-functionalized graphene surface in PBS for 1 hour at 4 °C or 37 °C by dipping and dropping the surfaces in cell suspensions, the control experiments included the incubation of cells with non-functionalized and PBA-functionalized graphene surfaces under the same conditions. After the incubation time, the surfaces were washed thoroughly with PBS solution several times. The cell binding

on the washed surfaces was analyzed via optical microscope or Raman spectrometer. The results are presented in Figure 4.5. As can be seen in the images, there was no interaction between the cells and the non-functionalized or PBA-functionalized graphene surface as expected. This indicated that there was no non-specific binding of Jurkat cells to the graphene surfaces. For Ab-functionalized surfaces, it was observed that Jurkat cells adhered to the graphene surface on antiCD2 functionalized surfaces at 4 °C. Considering this result, the use of 4 °C for incubation of cells with Ab-functionalized surfaces was found to be suitable for further experiments.

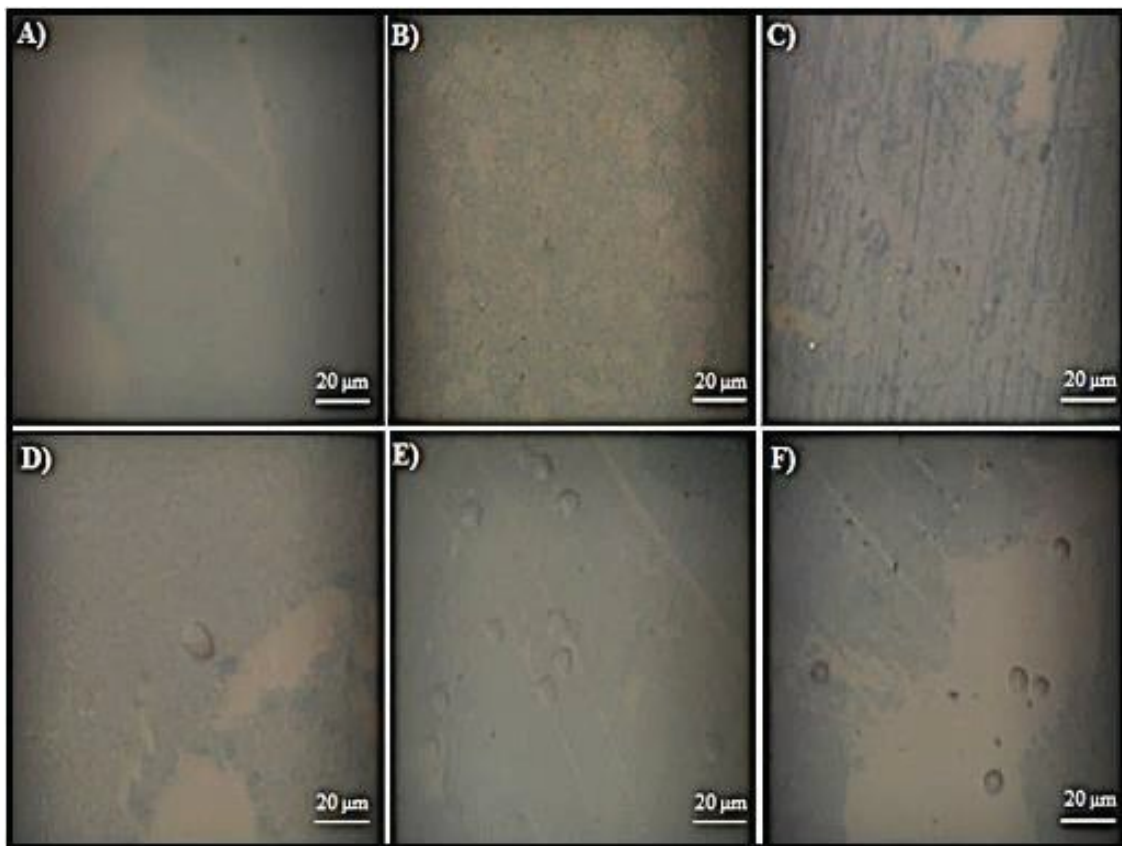


Figure 4.5. Effect of temperature on cell interaction with graphene surfaces in PBS for 1 hour by dipping method. Optical microscope images of (A) nonfunctionalized graphene surface after interaction with cells at 4° C, (B) nonfunctionalized graphene surface after interaction with cells at 37° C, (C) PBA-functionalized graphene surface after interaction with cells at 4° C, (D) PBA-functionalized graphene surface after interaction with cells at 37° C, (E) Ab-conjugated graphene surface after interaction with cells at 4° C, (F) Ab-conjugated graphene surface after interaction with cells at 37° C.

Secondly, the interaction method was investigated. The cells were interacted with the surface either by dipping the surfaces in cell suspension or by dropping the cell suspension onto the surfaces. In these experiments, cells were suspended in PBS and

incubated with surfaces at 4 °C for 1 hour. The results are presented in Figure 4.6. As it can be seen in the images, the cell binding was most significant when the cells were incubated with Ab-functionalized surfaces via dipping method. The number of cells recognized and attached to the surface was the highest when the Ab-functionalized surfaces were immersed into the cell suspension.

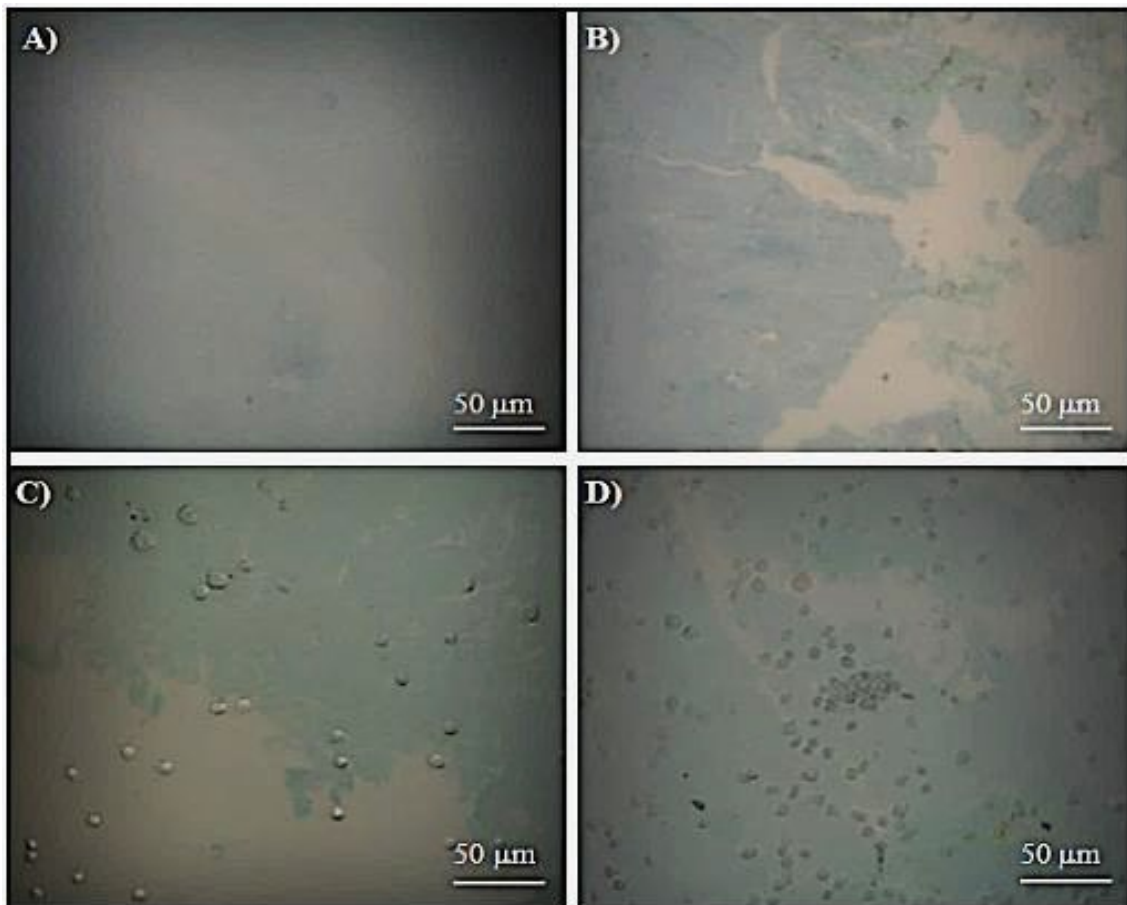


Figure 4.6. Effect of method on cell interaction with graphene surfaces in PBS at 4°C for 1 hour. Optical microscope images of (A) PBA-functionalized graphene surface after interaction with cells via dropping method, (B) PBA- functionalized graphene surface after interaction with cells via dipping method, (C) Ab-conjugated graphene surface after interaction with cells by dropping method, (D) Ab-conjugated graphene surface after interaction with cells by dipping method.

At the next step, the effect of medium on the cell-surface interaction was investigated. The cells were interacted with the surfaces in either PBS or cell culture medium at 4 °C via dipping method for 1 hour. The results are presented in Figure 4.7. As it can be seen in the images, the cell binding was most significant when the cells were incubated with Ab-functionalized surfaces in PBS. It is possible that the proteins and

other constituents of the cell culture medium non-specifically adsorb on the Ab-functionalized graphene surfaces and inhibit the specific recognition and attachment of Jurkat cells onto the antiCD2 antibodies on the graphene surfaces. Based on the result of this experiment, PBS was found to provide a better environment of cell-surface interaction.

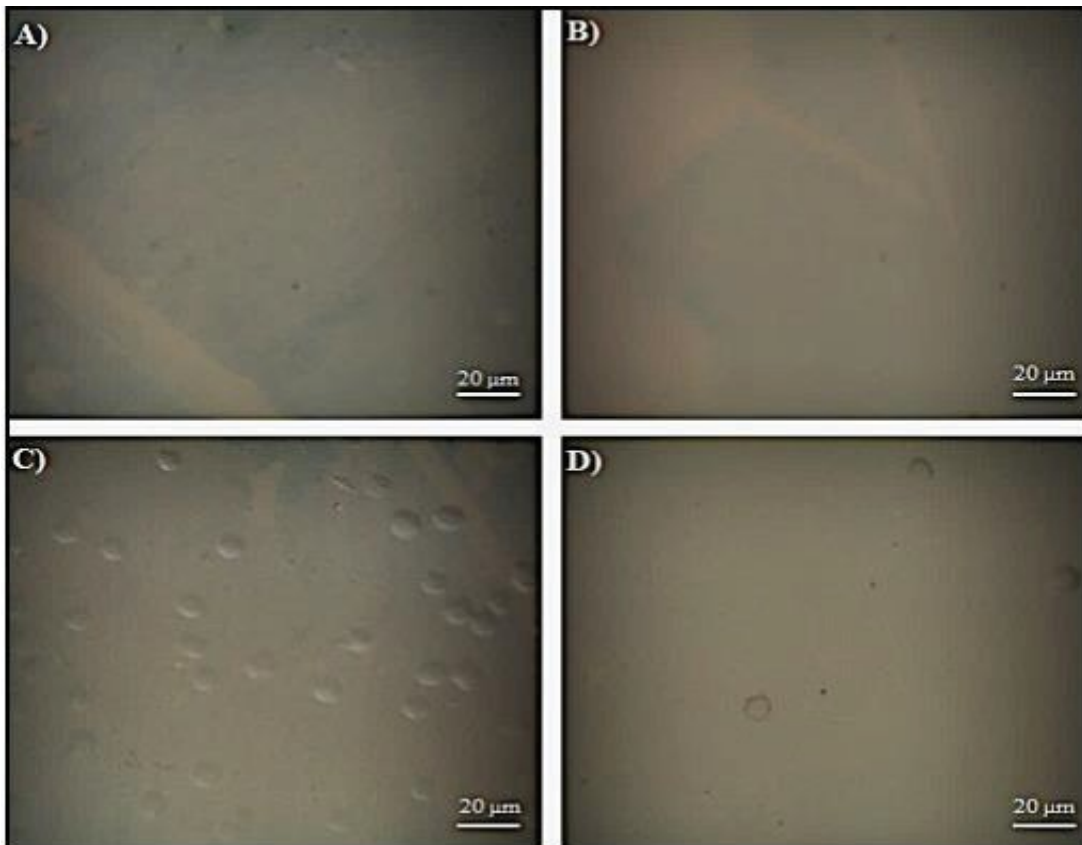


Figure 4.7. Effect of medium on cell interaction with graphene surfaces at 4°C for 1 hour via dipping method. Optical microscope images of (A) PBA-functionalized graphene surface after interaction with cells in PBS, (B) PBA-functionalized graphene surface after interaction with cells in cell culture medium, (C) Ab-conjugated graphene surface after interaction with cells in PBS, (D) Ab-conjugated graphene surface after interaction with cells in cell culture medium.

Overall the results of the above-given experiments showed that the specific recognition and attachment of Jurkat cells onto the antiCD2 antibody-functionalized surfaces were obtained when the cells were interacted with the antibody-conjugated surfaces in PBS at 4 °C via dipping method. Using these conditions, the specificity of the antiCD2 Ab-functionalized surfaces against Jurkat cells was also investigated. In this experiment, a non-specific antibody, mouse anti-Syndecan-1 that being a monoclonal

antibody was conjugated to the PBA-functionalized graphene surfaces following the same experimental conjugation procedure using NHS/EDC chemistry. There is no receptors specific to mouse anti-Syndecan-1 antibodies on Jurkat cells. It was therefore anticipated that there would be no recognition of the Anti-Syndecan-1 antibody conjugated surfaces by Jurkat cells. Figure 4.8 shows the optical microscopy images of the anti-Syndecan-1 antibody conjugated surfaces after incubation with Jurkat cells in PBS at 4 °C for 1 hour via dipping method. As it can be seen, the Jurkat cells did not recognize and attach onto the non-specific antibody conjugated surfaces while the cells attached efficiently onto the antiCD2 antibody-conjugated surfaces. This result directly proved that the recognition of Jurkat cells by the functionalized graphene surfaces was through specific antibody-surface receptor interactions.

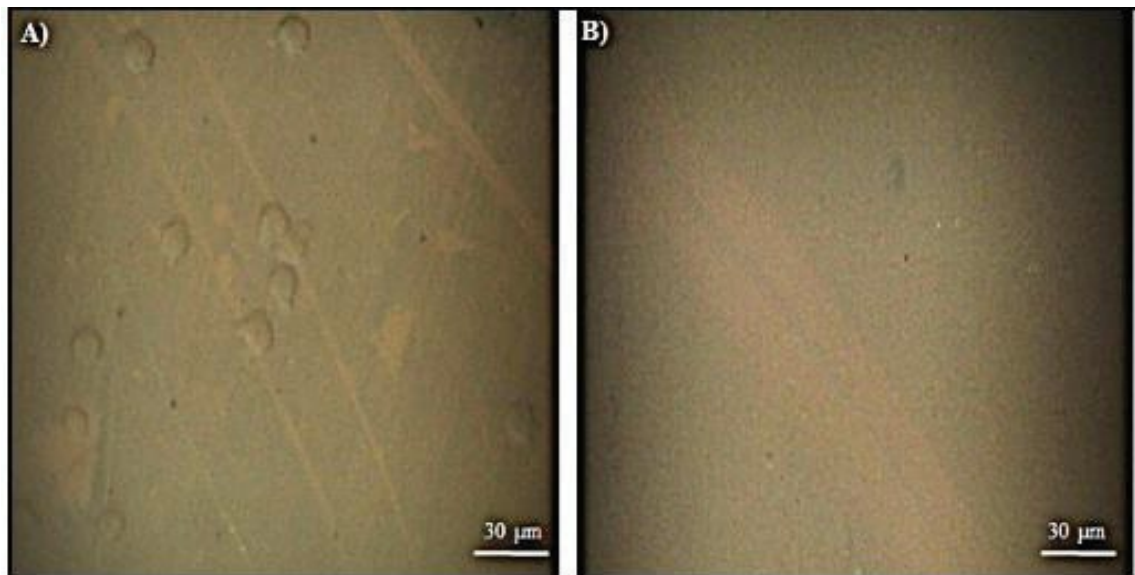


Figure 4.8. Optical microscope images of (A) antiCD2 antibody-conjugated graphene surface after interaction with Jurkat cells in PBS at 4°C for 1 hour via dipping method, (B) Anti-Syndecan-1 antibody-conjugated graphene surface after interaction with Jurkat cells in PBS at 4°C for 1 hour via dipping method.

In the last step, new experiment was designed to further show that the Jurkat cell- antiCD2 antibody-functionalized graphene surface interactions were through the specific antibody-surface receptor interactions. The cell-bound surfaces were incubated with the excess of antiCD2 antibodies and the surfaces were analyzed by optical microscopy to see whether the cells were remained on the surfaces or not. In this experiment, cells were first incubated with the antiCD2 conjugated surface at the

optimized conditions. After washing step, the cell-bound surface was treated with a solution of antiCD2 antibody (30

$\mu\text{g/ml}$  in PBS) for 1 hour and then analyzed via optical microscopy (Figure 4.9). Surface-bound cells were clearly observed on antiCD2 antibody-functionalized graphene surface after before treatment with high concentrations of antiCD2 antibody solution. When these surfaces were interacted with a high concentration of antibody solution, no cells were observed on the graphene surface. Since the cell surface receptors would have the same or higher affinity towards the antiCD2 antibodies in solution, the attachment of cells onto the surface-bound antibodies would be expected to be replaced by antiCD2 antibodies in solution, which would lead to the release of the surface-adhered cells into the solution.

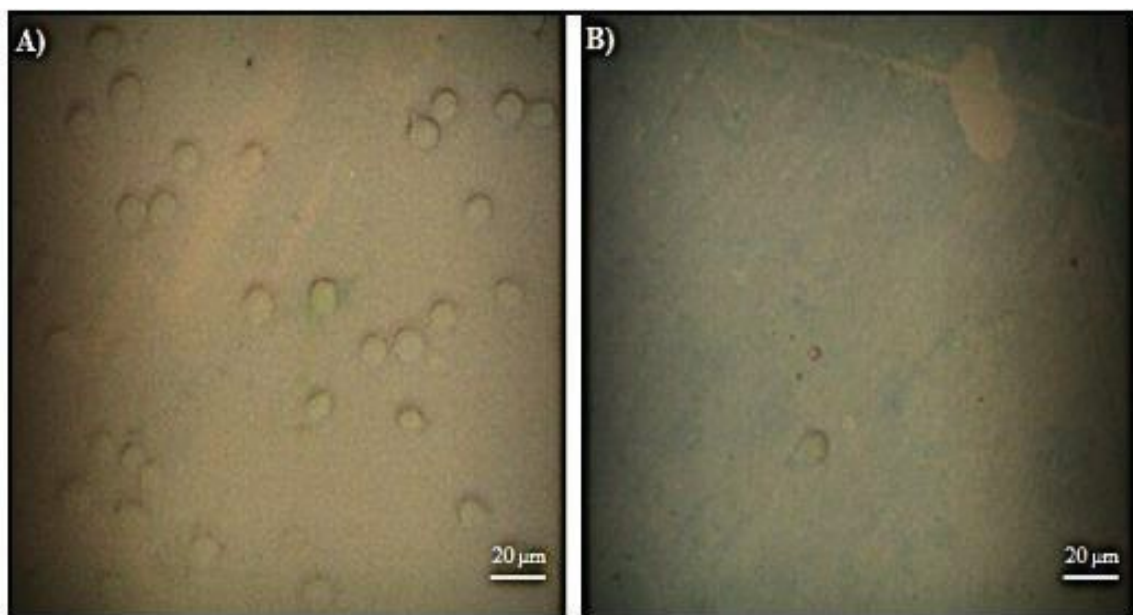


Figure 4.9. Optical microscope images of antiCD2 antibody-conjugated graphene surfaces after interaction with Jurkat cells followed by the treatment with the antiCD2 antibody solution ( $30 \mu\text{g/ml}$  in PBS) for 1 hour at  $4^\circ\text{C}$ . (A) Before and (B) after treatment with the excess of antiCD2 antibody solution.

## CHAPTER 5

### CONCLUSION

This thesis aims to prepare a graphene-based biosensor substrate for detection of biomicroparticles such as bacteria, viruses or mammalian cells. For this aim, it was first attempted to optimize the functionalization of graphene surfaces with PBA. The effect of solvent type on graphene surface functionalization was investigated by Raman spectroscopy and X-Ray spectroscopy (XPS). Appropriate solvent was determined as methanol when the results obtained were evaluated.

Graphene surface-antibody interaction was then investigated.. AntiCD2 antibodies (Ab) as a model antibody were interacted with the functionalized graphene surface via EDC/NHS chemistry. Biomolecule conjugation was examined and confirmed using Raman spectroscopy and XPS. Optimum parameters were determined to be the optimum medium and optimum incubation time for graphene surface-antibody conjugation were found to be MES buffer and 6h according to XPS and raman results for antibody conjugation to graphene surface.

Jurkat cells, a non-adherent cell line, were recognized by Ab-activated graphene surface and cell attachment was observed by optical microscopy. Temperature, medium and the method for interaction of cells with Ab-functionalized graphene surfaces were investigated. According to these investigations, the optimum temperature and the medium for cell-surface interaction were found to be 4 °C and PBS. It was also determined that dipping method was the more appropriate method for cell-surface interaction when compared with dropping method. Furthermore, the cell-surface interaction proved to be through specific Ab-cell receptor interactions as a non-specific Ab-, anti-Syndecan-1 antibodies, functionalized graphene surface did not recognize and capture Jurkat cells. More importantly, upon exposure of the cell-attached graphene surface to a high- concentration of antiCD2 antibodies, the cells were observed to be released from the graphene surface, evidencing that the cell attachment to the graphene surface was through the affinity binding between antiCD2 antibodies on the graphene

surface and CD2 receptors on the cell membrane. Overall, this thesis provided a method optimized for

preparation of Ab-functionalized graphene-based substrate for recognition of nonadherent mammalian cells through their specific surface receptors.

## **FUTURE WORKS**

The studies performed in this thesis can be further extended to include the following investigations:

1. Characterization of cell binding to the functionalized graphene surface needs to be performed using a technique other than optical microscopy. For example, fluorescence microscopy can be used after staining the cells on the surface. Also Raman spectroscopy can be used to indicate the attachment of cells on the surface.
2. Antibody density on the surface can be characterized and varied to enhance the number of cells recognized by the graphene surface.
3. The developed biochips can be integrated to a biosensor system to create a diagnostic tool.

## REFERENCES

1. Kroto, H. W.; Heath, J. R.; O'Brien, S. C.; Curl, R. F.; Smalley, R. E. Buckminsterfullerene, *Nature*, **1985**, *60* (318), 162-163.
2. Iijima, S. Helical Microtubules of Graphitic Carbon. *Nature*, **1991**, *354*, 56-58.
3. Sharon, M.; Graphene, M. *An Introduction to the Fundamentals and Industrial Applications*. John Wiley & Sons, Inc., Hoboken. 2015.
4. Novoselov, K. S., Geim, A. K.; Morozov, S. V.; Jiang, D.; Zhang, Y.; Dubonos, S. V.; Gregorieva, I. V.; Firsov, A. A. Electric Field Effect in Atomically Thin Carbon Films, *Science*, **2004**, *306*(5696), 666-669.
5. Zhu, Y.; Murali, S.; Cai, W.; Li, X.; Suk, J. W.; Potts, J. R.; Ruoff, R. S. Graphene and Graphene Oxide: Synthesis, Properties, and Applications, *Advanced Materials*, **2010**, *22*, 3906-3924.
6. Choi, W.; Lee, J. *Graphene: Synthesis and Applications*. CRC Press: Boca Raton. 2012.
7. Das, S.; Sudhagar, P.; Kang, Y.S.; Choi, W.; Synthesis and Characterization of Graphene. In: *Carbon Nanomaterials for Advanced Energy Systems*, Lu, W., Baek, J.; Dai, L., Eds., John Wiley & Sons, Inc., Hoboken, NJ, 2015, pp 85-131.
8. Lee, C.; Wei, X.; Kysar, J.W.; Hone, J. Measurement of the Elastic Properties and Intrinsic Strength of Monolayer Graphene. *Science*, **2008**, *321*, 385-388.
9. Morozov, S. V.; Novoselov, K. S.; Katsnelson, M. I.; Schedin, F.; Elias, D. C.; Jaszczak, J. A.; Geim, A. K. Giant Intrinsic Carrier Mobilities in Graphene and Its Bilayer. *Physical Review Letters*, **2008**, *100*.
10. Bolotin, K. I.; Sikes, K. J.; Jiang, Z.; Klima, M.; Fudenberg, G.; Hone, J.; Stormer, H. L. Ultrahigh Electron Mobility in Suspended Graphene. *Solid State Communications*, *146*(9-10), **2008**, 351-355.

11. Balandin, A. A.; Ghosh, S.; Bao, W.; Calizo, I.; Teweldebrhan, D.; Miao, F.; Lau, C. N. Superior Thermal Conductivity of Single-Layer Graphene. *Nano letters*, 8(3), **2008**, 902-907.
12. Moser, J.; Barreiro, A.; Bachtold, A. Current-Induced Cleaning of Graphene. *Applied Physics Letters*, **2007**, 91,
13. Kozlov, S.M.; Viñes, F.; Görling, A. Bandgap Engineering of Graphene by Physisorbed Adsorbates. *Advanced Materials*, **2011**, 23, 2638-2643.
14. Lonkar, S.P.; Deshmukh, Y. S.; Abdala, A. A. Recent Advances In Chemical Modifications of Graphene: A review. *Nano Research*, **2015**, 8(4), 1039–1074.
15. Geim, A. K.; Novoselov, K. S. The Rise of Graphene. *Nature Materials*, **2007**, 6, 183–191.
16. Novoselov, K. S.; Geim, A. K.; Morozov, S. V.; Jiang, D.; Zhang, Y.; Dubonos, S. V.; Grigorieva, I. V.; Firsov, A. A. Electric Field Effect in Atomically Thin Carbon Films. *Science*, **2004**, 306, p: 666–669.
17. Wei, D.; Liu, Y.; Wang, Y.; Zhang, H.; Huang, L.; Yu, G. Synthesis of N-Doped Graphene by Chemical Vapor Deposition and Its Electrical Properties. *Nano Letters*, **2009**, 9, 1752-1758.
18. Seyller, T.; Bostwick, A.; Emtsev, K. V.; Horn, K.; Ley, L.; McChesney, J. L.; Ohta, T.; Riley, J. D.; Rotenberg, E.; Speck, F. *Phys. Status Solidi B* **2008**, 245, 1436–1446.
19. Paredes, J.I.; Villar-Rodil, S.; Solís-Fernández, P.; Martínez-Alonso, A.; Tascón, J.M.D. Atomic Force and Scanning Tunneling Microscopy Imaging of Graphene Nanosheets Derived from Graphite Oxide. *Langmuir*, **2009**, 25, 5957-5968.
20. Park, S.; Ruoff, R.S. Chemical Methods for the Production of Graphenes. *Nature Nanotechnology*, **2009**, 4, 217-224.
21. Allen, M.J.; Tung, V.C.; Kaner, R.B. Honeycomb Carbon: A Review of Graphene. *Chemical Reviews*, **2010**, 110, 132-145.
22. Viculis, L.M.; Mack, J.J.; Kaner, R.B. A Chemical Route to Carbon Nanoscrolls. *Science*, **2003**, 299, 1361.

23. Rollings, E.; Gweon, G.-H.; Zhou, S. Y.; Mun, B. S.; McChesney, J. L.; Hussain, B. S.; Fedorov, A. V.; First, P. N.; de Heer, W. A.; Lanzar, A. Synthesis and characterization of atomically thin graphite films on a silicon carbide substrate, *J. Phys. Chem. Solids*, **2006**, 67, 2172–2177.
24. Reina, A.; Jia X. T; Ho J, Nezich. D.; Son, H. B.; Bulovic V; Dresselhaus. M. S.; Kong, J. Layer Area, Few-Layer Graphene Films on Arbitrary Substrates By Chemical Vapor Deposition, *Nano Lett.* **2009**, 9, 30-35.
25. Liu, N.; Luo, F.; Wu, H.; Liu, Y.; Zhang, C.; Chen, J. One-Step Ionic- Liquid-Assisted Electrochemical Synthesis of Ionic-Liquid-Functionalized Graphene Sheets Directly from Graphite. *Advanced Functional Materials*, **2008**, 18, 1518-1525.
26. Xin, G.; Hwang, W.; Kim, N.; Cho, S.M.; Chae, H. A. Graphene Sheet Exfoliated with Microwave Irradiation and Interlinked by Carbon Nanotubes for High-Performance Transparent Flexible Electrodes. *Nanotechnology*, **2010**, 21.
27. Jiao, L.; Wang, X.; Diankov, G.; Wang, H.; Dai, H. Facile Synthesis of High-Quality Graphene Nanoribbons. *Nature Nanotechnology*, **2010**, 5, 321-325.
28. Kosynkin, D. V.; Higginbotham, A. L.; Sinitskii, A.; Lomeda, J. R.; Dimiev, A.; Price, B. K.; Tour, J. M. Longitudinal Unzipping of Carbon Nanotubes to Form Graphene Nanoribbons. *Nature*, **2009**, 458 (7240), 872-876.
29. Jiao, L.; Zhang, L.; Wang, X.; Diankov, G.; Dai, H. Narrow Graphene Nanoribbons from Carbon Nanotubes. *Nature*, **2009**, 458, 877-880.
30. Ebbesen, T.W.; Hiura, H. Graphene in 3-Dimensions: Towards Graphite Origami. *Advanced Materials*, **1995**, 7, 582-586.
31. Lu, X.; Yu, M.; Huang, H.; Ruoff, R.S. Tailoring Graphite with the Goal of Achieving Single Sheets. *Nanotechnology*, **1999**, 10, 269-272.
32. Lang, B. A LEED Study of the Deposition of Carbon on Platinum Crystal Surfaces. *Surface Science*, **1975**, 53, 317-329.

33. Liang, X.; Chang, A. S.; Zhang, Y.; Harteneck, B. D.; Choo, H.; Olynick, D. L.; Cabrini, S. Electrostatic Force Assisted Exfoliation of Prepatterned Few-Layer Graphenes into Device Sites. *Nano letters*, **2008**, 9(1), 467-472.
34. Ci, L.; Song, L.; Jariwala, D.; Elias, A. L.; Gao, W.; Terrones, M.; Ajayan, P. M. Graphene Shape Control by Multistage Cutting and Transfer. *Advanced Materials*, **2009**, 21(44), 4487-4491.
35. Rao, C.N.R.; Sood, A.K. *Graphene: Synthesis, Properties, and Phenomena*. John Wiley & Sons, Inc., Weinheim, Germany, 2013.
36. Viculis, L.M.; Mack, J.J.; Mayer, O.M.; Hahn, H.T.; Kaner, R.B. Intercalation and Exfoliation Routes to Graphite Nanoplatelets. *Journal of Materials Chemistry*, **2005**, 15, 974-978.
37. Bhuyan, M.S.A.; Uddin, M.N.; Islam, M.M.; Bipasha, F.A.; Hossain, S.S. Synthesis of Graphene. *International Nano Letters*, **2016**, 6, 65-83.
38. Van Bommel, A.J.; Crombeen, J.E.; Van Tooren A. LEED and Auger Electron Observations of the SiC (0001) Surface. *Surface Science*, **1975**, 48, 463-472.
39. Berger, C.; Song, Z. M.; Li, T. B.; Li, X. B.; Ogbazghi, A. Y.; Feng, R.; Dai, Z. T.; Marchenkov, A. N.; Conrad, E. H.; First, P. N.; de Heer, W. A. Ultrathin Epitaxial Graphite: 2D Electron Gas Properties and A Route Toward Graphene-Based Nanoelectronics. *J. Phys. Chem B*, **2004**, 108 (52), 19912–19916.
40. De Heer, W. A.; Berger, C.; Wu, X. S.; First, P. N.; Conrad, E. H.; Li, X. B.; Li, T. B.; Sprinkle, M.; Hass, J.; Sadowski, M. L.; Potemski, M.; Martinez, G. Epitaxial Graphene. *Solid State Commun.* **2007**, 143, 92-100.
41. Juang, Z. Y.; Wu, C. Y.; Lo, C. W.; Chen, W. Y.; Huang, C. F.; Hwang, J.C.; Chen, F.R.; Leou, K.C.; Tsai, C.H. Synthesis of Graphene on Silicon Carbide Substrates at Low Temperature. *Carbon*, **2009**, 47, 2026-2031.
42. Guo, S.; Dong, S.; Wang, E. Three-Dimensional Pt-On-Pd Bimetallic Nanodendrites Supported on Graphene Nanosheet: Facile Synthesis and Used as an Advanced Nanoelectrocatalyst for Methanol Oxidation. *ACS Nano*, **2010**, 4, 547-555.

43. Sutter, P. W.; Flege, J. I.; Sutter, E. A. Epitaxial Graphene on Ruthenium, *Nature Materials*, **2008**, 7, 406-411.
44. Coraux, J.; N'Diaye, A.T.; Busse, C.; Michely, T. Structural Coherency of Graphene on Ir (111). *Nano Letters*, **2008**, 8, 565-570.
45. Karu, A.E.; Beer, M. Pyrolytic Formation of Highly Crystalline Graphite Films. *Journal of Applied Physics*, **1966**, 37, 2179-2181.
46. Perdereau, J.; Rhead, G.E. LEED Studies of Adsorption on Vicinal Copper Surfaces. *Surface Science*, **1971**, 24, 555-571.
47. Eizenberg, M.; Blakely, J.M. Carbon Monolayer Phase Condensation on Ni (111). *Surface Science*, **1979**, 82, 228-236.
48. Lee, J.; Zheng, X.; Roberts, R.C.; Feng, P.X.L. Scanning Electron Microscopy Characterization of Structural Features in Suspended and Non-Suspended Graphene by Customized CVD Growth. *Diamond and Related Materials*, **2015**, 54, 64-73.
49. Karousis, N.; Sandanayaka, A. S. D.; Hasobe, T.; Economopoulos, S. P.; Sarantopoulou, E.; Tagmatarchis, N. Graphene Oxide with Covalently Linked Porphyrin Antennae: Synthesis, Characterization and Photophysical Properties. *Journal of Materials Chemistry*. **2011**, 21, 109–117.
50. Liu, Z. B.; Xu, Y. F.; Zhang, X. Y.; Zhang, X. L.; Chen, Y.S.; Tian, J. G. Porphyrin and fullerene covalently functionalized graphene hybrid materials with large nonlinear optical properties. *The Journal of Physical Chemistry B*, **2009**, 113, 9681–9686.
51. Long, F.; Zhu, A. N.; Shi, H. C.; Wang, H. C. Hapten Grafted Graphene as A Transducer for Homogeneous Competitive Immunoassay of Small Molecules. *Analytical Chemistry*. **2014**, 86, 2862–2866.
52. Yang, H. F.; Li, F. H.; Shan, C. S.; Han, D. X.; Zhang, Q. X.; Niu, L.; Ivaska, A. Covalent Functionalization of Chemically Converted Graphene Sheets Via Silane and Its Reinforcement. *Journal of Materials Chemistry*, **2009**, 19, 4632–4638.

53. Mann, J. A.; Dichtel, W. R. Noncovalent Functionalization of Graphene By Molecular and Polymeric Adsorbates. *The Journal of Physical Chemistry*, **2013**, *4*, 2649–2657.
54. Parviz, D.; Das, S.; Ahmed, H. S. T.; Irin, F.; Bhattacharia, S.; Green, M. J. Dispersions of Non-Covalently Functionalized Graphene with Minimal Stabilizer. *ACS Nano*, **2012**, *6*, 8857–8867.
55. Basiuk, E. V.; Martinez-Herrera, M.; Alvarez-Zauco, E.; Henao-Holguin, L. V.; Puente-Lee, I.; Basiuk, V. A. Noncovalent Functionalization of Graphene with A Ni (II)Tetraaza Annulene Complex. *Dalton Transactions*, **2014**, *43*, 7413–7428.
56. Coluci, V. R.; Martinez, D. S. T.; Honorio, J. G.; de Faria, A. F.; Morales, D. A.; Skaf, M. S.; Alves, O. L.; Umbuzeiro, G. A. Noncovalent Interaction With Graphene Oxide: The Crucial Role of Oxidative Debris. *The Journal of Physical Chemistry C*, **2014**, *118*, 2187–2193.
57. Qu, S. X.; Li, M. H.; Xie, L. X.; Huang, X.; Yang, J. G.; Wang, N.; Yang, S. F. Noncovalent Functionalization of Graphene Attaching [6,6]-Phenyl-C61-Butyric Acid Methyl Ester (Pcbm) and Application as Electron Extraction Layer of Polymer Solar Cells. *ACS Nano*, **2013**, *7*, 4070–4081.
58. Lee, D. Y.; Khatun, Z.; Lee, J. H.; Lee, Y. K.; In, I. Blood Compatible Graphene/Heparin Conjugate Through Noncovalent Chemistry. *Biomacromolecules*, **2011**, *12*, 336–341.
59. Yang, Q.; Pan, X. J.; Huang, F.; Li, K. C. Fabrication of High-Concentration and Stable Aqueous Suspensions of Graphene Nanosheets by Noncovalent Functionalization with Lignin and Cellulose Derivatives. *The Journal of Physical Chemistry C*, **2010**, *114*, 3811–3816.
60. Chen, X. J.; Yasin, F. M.; Eggers, P. K.; Boulos, R. A.; Duan, X. F.; Lamb, R. N.; Iyer, K. S.; Raston, C. L. Noncovalently Modified Graphene Supported Ultrafine Nanoparticles of Palladium for Hydrogen Gas Sensing. *RSC Advances*, **2013**, *3*, 3213–3217.
61. Ager, A., *Immunology Today. Immune receptor supplement*, Cambridge: Elsevier Trends Journals. 1996.
62. Davies, D.R.; S. Chacko, Antibody Structure. *Accounts of Chemical Research*, **1993**, *26*(8), 421-427.

63. Schroeder, H. W.; Cavacini, L. Structure and Function of Immunoglobulins. *Journal of Allergy and Clinical Immunology*, **2010**, *125*(2), 41-52.
64. Garcia, K.C.; Teyton, L.; Wilson, I.A.; Structural Basis of T-Cell Recognition. *Annual Review of Immunology*, **1999**, *17*(1), 369-397.
65. Amzel, L. M.; Poljak, R. J. A. Three-Dimensional Structure of Immunoglobulins. *Annual Review of Biochemistry*, **1979**, *48*(1), 961-997.
66. Harris, L. J.; Larson, S. B.; Hasel, K. W.; Day, J.; Greenwood, A.; McPherson, A. The Three-Dimensional Structure of An Intact Monoclonal Antibody for Canine Lymphoma. *Nature*, **1992**, *360*(6402), 369-372.
67. Germain, R.N., MHC-Dependent Antigen Processing and Peptide Presentation: Providing Ligands for T Lymphocyte Activation. *Cell*, **1994**, *76*(2), 287-299.
68. Edelman, G. M. Antibody Structure and Molecular Immunology. *Scandinavian Journal of Immunology*, **1991**, *34*(1), 4-22.
69. Han, W.; Mou, J.; Sheng, J.; Yang, J.; Shao, Z. Cryo Atomic Force Microscopy: A New Approach for Biological Imaging at High Resolution. *Biochemistry*, **1995**, *34*(26), 8215-8220.
70. Wu, T. T.; Kabat, E. A. An Analysis of Sequences of The Variable Regions of Bence Jones Proteins and Myeloma Light Chains and Their Implications for Antibody Complementarity, *The Journal of Experimental Medicine*, **1970** *132*(2), 211-250.
71. Yamaguchi, Y.; Kim, H.; Kato, K.; Masuda, K.; Shimada, I.; Arata, Y. Proteolytic Fragmentation With High Specificity of Mouse Immunoglobulin G Mapping of Proteolytic Cleavage Sites in The Hinge Region. *Journal of Immunological Methods*, **1995**, *181*(2), 259-267.
72. Yamaguchi, Y.; Kim, H.; Kato, K.; Masuda, K.; Shimada, I.; Arata, Y. Proteolytic Fragmentation with High Specificity of Mouse Immunoglobulin G Mapping of Proteolytic Cleavage Sites in The Hinge Region. *Journal of Immunological Methods*, **1995**, *181*(2), 259-267.

73. Chitarra, V.; Alzari, P. M.; Bentley, G. A.; Bhat, T. N.; Eisele, J. L.; Houdusse, A.; Lescar, J.; Souchon, H.; Poljak, R. J. Three-Dimensional Structure of A Heteroclitic Antigen-Antibody Cross-Reaction Complex. *Proceedings of the National Academy of Sciences of the United States of America*, **1993**, 90(16) 7711-7715.
74. Yamaguchi, Y.; Kim, H.; Kato, K.; Masuda, K.; Shimada, I.; Arata, Y. Proteolytic Fragmentation With High Specificity of Mouse Immunoglobulin G Mapping of Proteolytic Cleavage Sites in The Hinge Region. *Journal of Immunological Methods*, **1995**, 181(2), 259-267.
75. Conte, L.L.; Chothia, C.; Janin, J. The Atomic Structure of Protein-Protein Recognition Sites11Edited by A. R. Fersht. *Journal of Molecular Biology*, **1999**, 285(5), 2177-2198.
76. Hinnemo, M.; Zhao, J.; Ahlberg, P.; Hägglund, C.; Djurberg, V.; Scheicher, R.H.; Zhang, S. L.; Zhang, Z. B. On Monolayer Formation of Pyrenebutyric Acid on Graphene. *Langmuir*; **2017**, 33, 3588-3593.
77. Singh, M.; Holzinger, M.; Tabrizian, M.; Winters, S.; Berner, N. C.; Cosnier, S.; Duesberg, G. S. Noncovalently Functionalized Monolayer Graphene for Sensitivity Enhancement of Surface Plasmon Resonance Immunosensors *J. Am. Chem. Soc.* **2015**, 137, 2800– 2803.
78. Smith, E.; Dent, G. *Modern Raman Spectroscopy - A Practical Approach*, Wiley, 2005.
79. Patel S. K. S.; Anwar M. Z.; Kumar, A.; Otari S. V.; Pagolu R. T.; Kim, S. Y.; Kim, I. W.; Lee. J. K. Fe<sub>2</sub>O<sub>3</sub> Yolk Shell Particle Based Laccase Biosensor for Efficient Detection of 2,6 Dimethoxyphenol. *Biochem Eng J.* **2018**, 132, 1–8.
80. Ye, Y.; Xie J.; Ye, Y.; Cao, X.; Zheng, H.; Xu, X.; Zhang, Q. A Label-Free Electrochemical Dna Biosensor Based on Thionine Functionalized Reduced Graphene Oxide. *Carbon*, **2018**, 129, 730–737.
81. Haque, R.; Kress, K.; Wood, S.; Jackson, T. F.; Lyerly, D.; Wilkins, T.; Petri, Jr, W. A. Diagnosis of Pathogenic Entamoeba Histolytica Infection Using A Stool Elisa Based on Monoclonal Antibodies to The Galactose-Specific Adhesin. *Journal of Infectious Diseases*, **1993**, 167(1), 247-249.

82. Morales-Narváez E.; Baptista-Pires L.; Zamora-Gálvez, A.; Merkoçi, A.; Graphene-Based Biosensors: Going simple. *Adv Mater.* **2017**, *29*(7), 1604905.
83. Chauhan, N.; Maekawa, T.; Kumar, D.N.S. Graphene Based Biosensors Accelerating Medical Diagnostics to New Dimensions. *J Mater Res.* **2017**, *32*, 2860–2882.
84. Park, C.S.; Yoon, H.; Kwon, O.S. Graphene Based Nanoelectronic Biosensors. *Journal of Industrial and Engineering Chemistry.* **2016**, *38*, 13–22.
85. Kuila, T.; Bose, S.; Khanra, P.; Mishra, A.K.; Kim, N.H.; Lee, J. H. Recent Advances in Graphene-Based Biosensors. *Biosens Bioelectron.* **2011**, *26*, 4637–48.
86. Huang, Y.; Dong, X.; Liu, Y.; Li, L.J.; Chen P. Graphene Based Biosensors for Detection of Bacteria and Their Metabolic Activities. *J Mater Chem,* **2011**, *21*, 12358.
87. Afsahi, S.; Lerner, M. B.; Goldstein, J. M.; Lee, J.; Tang, X.; Bagarozzi, D.A., Pan, D.; Locascia, L.; Walker, A.; Barron, F.; Goldsmith, B.R. Novel Graphene Based Biosensor for Early Detection of Zika Virus Infection. *Biosens Bioelectron.* **2018**, *100*, 85–88.
88. Thakur B.; Zhou, G.; Chang J.; Pu, H.; Jin, B.; Sui, X; Yuan, X.; Yang, C-H.; Magruder, M.; Chen, J. Rapid Detection of Single *E Coli* Bacteria Using A Graphene Based Field Effect Transistor Device. *Biosensor Bioelectron.* **2018**, *110*, 16–22.
89. Sign C.; Sumana G. Antibody Conjugated Graphene Nanocomposites for Pathogen Detection. *Journal of Physics,* **2016**, *704*, 7.
90. Bahamonde, J. P.; Nguyen, H. N.; Fanourakis, S. K.; Rodrigues, D. F. Recent Advances in Graphene-Based Biosensor Technology with Applications in Life Sciences. *Journal of nanobiotechnology,* **2018**, *16*(1), 75.